INFORMATION TO USERS

While the most advanced technology has been used to photograph and reproduce this manuscript, the quality of the reproduction is heavily dependent upon the quality of the material submitted. For example:

- Manuscript pages may have indistinct print. In such cases, the best available copy has been filmed.
- Manuscripts may not always be complete. In such cases, a note will indicate that it is not possible to obtain missing pages.
- Copyrighted material may have been removed from the manuscript. In such cases, a note will indicate the deletion.

Oversize materials (e.g., maps, drawings, and charts) are photographed by sectioning the original, beginning at the upper left-hand corner and continuing from left to right in equal sections with small overlaps. Each oversize page is also filmed as one exposure and is available, for an additional charge, as a standard 35mm slide or as a 17"x 23" black and white photographic print.

Most photographs reproduce acceptably on positive microfilm or microfiche but lack the clarity on xerographic copies made from the microfilm. For an additional charge, 35mm slides of 6"x 9" black and white photographic prints are available for any photographs or illustrations that cannot be reproduced satisfactorily by xerography.

8704762

Damento, Michael Anthony

DETECTION OF MAGNETIZATION REVERSAL IN A NEODYMIUM-IRON-BORON MAGNET USING A HALL-EFFECT MICROPROBE

The University of Arizona PH.D. 1986

University
Microfilms
International 300 N. Zeeb Road, Ann Arbor, MI 48106

PLEASE NOTE:

In all cases this material has been filmed in the best possible way from the available copy. Problems encountered with this document have been identified here with a check mark __✓__.

1. Glossy photographs or pages _____
2. Colored illustrations, paper or print _____
3. Photographs with dark background ✓
4. Illustrations are poor copy _____
5. Pages with black marks, not original copy _____
6. Print shows through as there is text on both sides of page _____
7. Indistinct, broken or small print on several pages _____
8. Print exceeds margin requirements _____
9. Tightly bound copy with print lost in spine _____
10. Computer printout pages with indistinct print _____
11. Page(s) _____ lacking when material received, and not available from school or author.
12. Page(s) _____ seem to be missing in numbering only as text follows.
13. Two pages numbered _____. Text follows.
14. Curling and wrinkled pages _____
15. Dissertation contains pages with print at a slant, filmed as received _____
16. Other _____

_____

_____

University
Microfilms
International

DETECTION OF MAGNETIZATION REVERSAL IN A Nd-Fe-B MAGNET USING A HALL-EFFECT MICROPROBE

by

Michael Anthony Damento

A Dissertation Submitted to the Faculty of the

DEPARTMENT OF MATERIALS SCIENCE AND ENGINEERING

In Partial Fulfillment of the Requirements
For the Degree of

DOCTOR OF PHILOSOPHY

In the Graduate College

THE UNIVERSITY OF ARIZONA

1 9 8 6

THE UNIVERSITY OF ARIZONA
GRADUATE COLLEGE

As members of the Final Examination Committee, we certify that we have read the dissertation prepared by Michael Anthony Damento

entitled Detection of Magnetization Reversal in a Nd-Fe-B Magnet Using a Hall-Effect Microprobe

and recommend that it be accepted as fulfilling the dissertation requirement for the Degree of Doctor of Philosophy.

Louis J. Demer	11-13-86 Date
Kenneth L. Kaplan	11-13-86 Date
Clyde M. Fowler	11-13-86 Date
S. Ray	11-14-86 Date
M. O. Scully	11-14-86 Date

Final approval and acceptance of this dissertation is contingent upon the candidate's submission of the final copy of the dissertation to the Graduate College.

I hereby certify that I have read this dissertation prepared under my direction and recommend that it be accepted as fulfilling the dissertation requirement.

Louis J. Demer	11-13-86
Dissertation Director	Date

STATEMENT BY AUTHOR

This dissertation has been submitted in partial fulfillment of requirements for an advanced degree at The University of Arizona and is deposited in the University Library to be made available to borrowers under rules of the Library.

Brief quotations from this dissertation are allowable without special permission, provided that accurate acknowledgment of source is made. Requests for permission for extended quotation from or reproduction of this manuscript in whole or in part may be granted by the head of the major department or the Dean of the Graduate College when in his or her judgment the proposed use of the material is in the interests of scholarship. In all other instances, however, permission must be obtained from the author.

SIGNED: Michael A. Damento

"For this stone not only attracts iron rings, but also imparts to them a power whereby they in turn are able to do the very same thing as the stone, and attract other rings; so that sometimes there is formed quite a long chain of bits of iron and rings, suspended from one another; and they all depend for this power on that one stone."

--Plato, **Ion**

ACKNOWLEDGMENTS

I am deeply indebted to my advisor, Dr. Louis Demer, for his support throughout my studies at the University of Arizona. By allowing me the freedom to explore, he made this work possible.

I owe special thanks to Dick Van Reeth for machine work and to Sal Gonzales for help with electrical design and materials. I would also like to thank David Keogel and Wang Ping for their many helpful suggestions.

Finally, I want to express my deepest appreciation to my wife, Evelyn, for her encouragement and to my mother, Carmetta Damento, for typing this dissertation.

TABLE OF CONTENTS

TABLE OF CONTENTS--Continued

LIST OF ILLUSTRATIONS

LIST OF ILLUSTRATIONS--Continued

LIST OF TABLES

ABSTRACT

Magnetization processes in a sintered Nd-Fe-B permanent magnet (NEOMAX-35) were examined on a small scale using a Hall-effect microprobe with an active area 75 μm on a side. Probes were made by evaporating bismuth through a stencil mask onto glass slides. Experiments were performed by placing a probe onto the polished pole face of a Nd-Fe-B magnet and inserting the probe-magnet assembly into an electromagnet. Barkhausen steps, indicating rapid domain wall motion, were observed (superimposed upon the blank probe signal) in the demagnetization of a fully magnetized magnet. Magnetization traces for a thermally demagnetized Nd-Fe-B magnet did not exhibit measurable Barkhausen steps until a field of approximately 1.2 T was applied. The following observations were made for two thermally demagnetized samples which were cycled through minor hysteresis loops (maximum applied field of approximately 2 T): (1) virgin magnetization traces did not contain measurable Barkhausen steps, however all other forward and reverse magnetization traces did; (2) the initial reverse magnetization trace exhibited more and larger Barkhausen steps than subsequent traces; and (3) some Barkhausen steps were repeatable, that is, occurring at approximately the same field on each

subsequent forward or reverse trace. Hall voltage signals were on the order of millivolts for probe currents of 10 mA.

CHAPTER 1

INTRODUCTION

Permanent magnets find use in a wide range of electromechanical devices such as motors, speakers, magnetic bearings and suspension systems, and medical devices. The figure of merit for a permanent magnet material is the maximum energy product, $(BH)_{max}$, defined as the maximum product of B and H in the second quadrant of the hysteresis loop (McCaig, 1977, p. 196). Materials with large $(BH)_{max}$ values are desirable from economic and size or weight limitation viewpoints since less material is needed for a given application. An historical record of the $(BH)_{max}$ values attained with various materials is presented in Fig. 1.

In the late 1960's a great achievement was made with the discovery of rare-earth cobalt permanent magnets (Hoffer and Strnat, 1966). The scarcity of cobalt and samarium which constituted the greater part of these magnets led to research into less expensive iron-rare-earth compounds with emphasis on the more common light rare-earth metals. This research led in 1982 to the discovery of the new Nd-Fe-B permanent magnets based on the hard magnetic compound $Nd_2Fe_{14}B$ (Sagawa and co-workers, 1984a). These magnets have the highest energy products currently attainable.

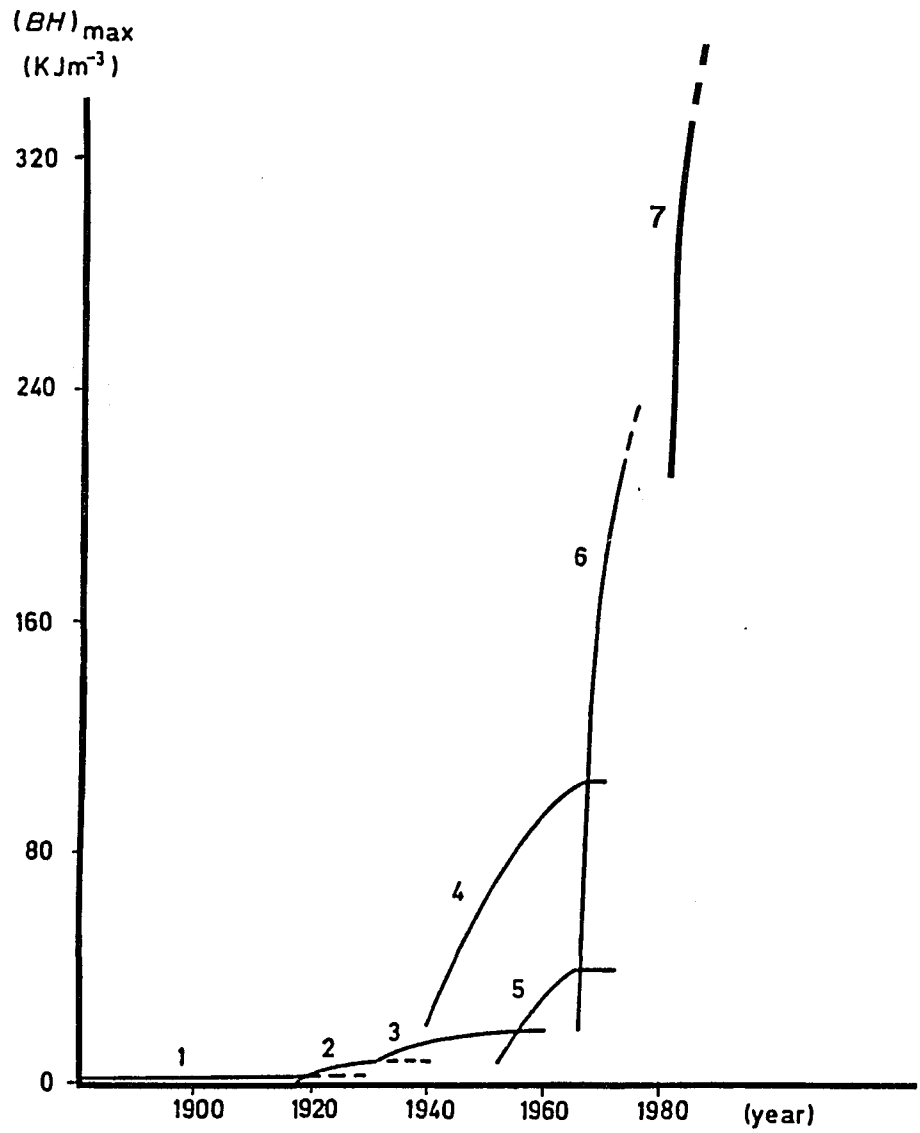

Fig. 1. Historical improvement of $(BH)_{max}$ of different classes of permanent magnets during the last hundred years. (1) Pre-cobalt steels. (2) Cobalt steels. (3) Isotropic Al-Ni-Co. (4) Anisotropic and columnar Al-Ni-Co. (5) Barium and strontium ferrite. (6) Rare-earth cobalt. (7) Nd-Fe-B. (From McCaig, 1977).

Also important in regard to the merit of a permanent magnet is the intrinsic coercivity or the resistance to demagnetization by external or self-imposed magnetic fields. In high-coercivity materials, domain walls are either prevented from moving (by pinning) or from being formed from the magnetically saturated state (nucleating). Studies on Nd-Fe-B magnets suggest that probably both mechanisms are important in this material. As one might guess, the actual observation (by electron or optical microscopy) of a nucleation event or a pinned wall is very difficult. Instead we must rely on inferences from observations made by various techniques.

The domain behavior in Nd-Fe-B magnets has been extensively studied in the past by electron microscopy (Hadjipanayis, Lawless, and Dickerson, 1985) and optical microscopy (Livingston, 1985, and Li and Strnat, 1985) employing the Kerr effect. Although these techniques involve direct observation of domain walls, in the case of the Kerr effect only surface domain structure is observed; and in electron microscopy only domain walls in very thin specimens can be studied. The relationship between domain behavior under these conditions and that in a bulk magnet is not completely clear. As an alternative and a supplement to the data obtained in those studies, a method of investigating magnetization changes in Nd-Fe-B on a microscopic scale using a Hall-effect microprobe was developed in the present

work. The application of this method to observations of domain-wall pinning is described herein.

CHAPTER 2

BACKGROUND

Ferromagnetism and Permanent Magnets

When a magnetic field, H, is applied to a ferromagnetic material, a magnetization per unit volume, M, is induced. As H is increased to large values, M is no longer increased and the material is said to be magnetically saturated. When H is returned to zero, M retains a positive value which can only be reduced to zero with the application of a reversed field, H_{ci} (intrinsic coercivity). A hysteresis loop thus develops as the material is cyclically magnetized and demagnetized (Fig. 2a).

Alternatively, the magnetic induction, B, can be plotted against H (Fig. 2b), where:

$$B = \mu_0(H+M), \qquad \text{Eq. 1}$$

and μ_0 is the permeability of free space ($4\pi\times10^{-7}$ Hm^{-1}). The remanent induction, B_r, and coercivity, H_c, are defined by Fig. 2b. Permanent magnets are rated in terms of a maximum energy product. It is defined as the maximum product of B and H in the second quadrant of the hysteresis loop.

Magnetic Domains

A piece of iron can be obtained in the demagnetized state because of the existence of domains. Within each

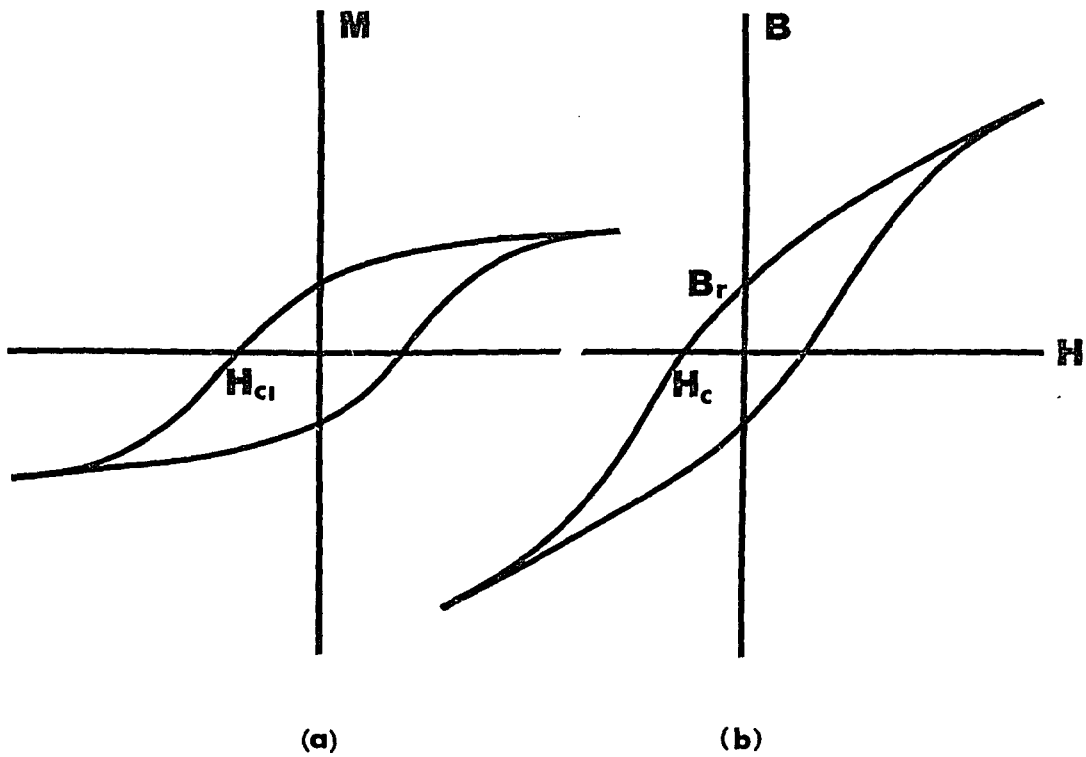

Fig. 2. Hysteresis loops for a ferromagnetic material. (a) Magnetization vs. applied field. (b) Induction vs. applied field.

domain the atomic magnetic moments tend to be aligned; however, adjacent domains can be arranged such that the net external field is minimized (Fig. 3). Energy is expended in creating the domain walls which separate adjacent domains (McCaig, 1977, p. 49). Consequently, the domain structure which is actually attained is one which minimizes the total energy of the system through a trade-off between the energy of the external magnetic field and the domain-wall energy.

The direction of spontaneous magnetization within a domain tends to lie along certain "easy" directions within a crystal. In iron (bcc), the directions of easy magnetization are <100> while those in nickel (fcc) are <111>. In cobalt (hcp) there is only one easy axis: [0001]. The magnetocrystalline energy per unit volume of a single crystal of a uniaxial ferromagnet such as cobalt is given by McCaig, (1977, p. 32):

$$E = K+K_1\sin^2\theta+K_2\sin^4\theta, \qquad \text{Eq. 2}$$

where θ is the angle between the magnetization direction and the easy axis, and K, K_1 and K_2 are empirical constants. If K_1 and K_2 are large for a given material, it becomes very difficult to rotate the magnetization vector away from the easy axis.

As a ferromagnetic material is magnetized (from the demagnetized state), the domain structure adjusts itself accordingly to retain a minimum energy configuration. This is shown schematically in Fig. 4. Initially, domains lying

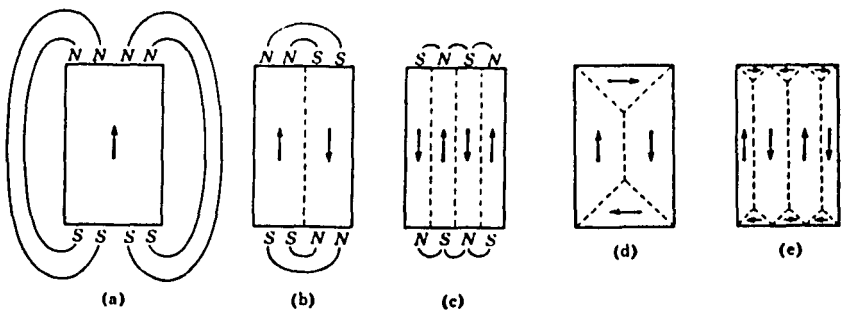

Fig. 3. The formation of domains in a single crystal of a ferromagnet. (From Kittel, 1976).

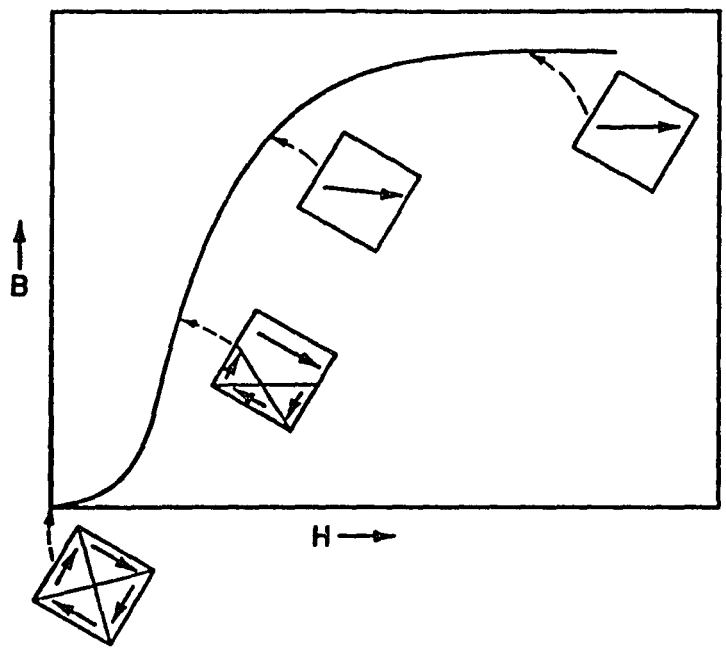

Fig. 4. Schematic illustration of domain structure at various stages of the magnetization process. (From Nesbitt and Wernick, 1973).

along easy axes which are favorably-oriented with the field grow at the expense of neighboring domains. This growth takes place by the movement of domain walls which separate the neighboring domains. In larger applied fields, the favorably oriented domain grows to consume the entire crystal, making it a single domain. Further increase in magnetization (in the direction of the applied field) occurs by the rotation of the magnetization vector in the direction of the applied field.

The hysteresis curves of Fig. 2 show that the movement of domain walls is not entirely reversible. Imperfections, impurities, and local stresses can pin domain walls until a large enough field is applied to break them free (McCaig, 1977, pp. 61-68). The remanent induction, B_r, which is observed after magnetizing a piece of iron or other ferromagnetic material is a result of domain walls being locked in place by defects within the grains or at grain boundaries.

Micromagnetics

The transition from one magnetization direction to another which occurs at a domain wall is not likely to take place across one interatomic spacing. The exchange energy which aligns the atomic magnetic moments is lower if the transition is gradual: neighboring atomic-magnetic-moment vectors making a small angle with each other between domains

(Kittel, 1976, p. 488). The result is that domain walls have a finite width. Domain walls in a ferromagnetic crystal with a large anisotropy constant will be narrow because rotation of the magnetization vector is very difficult. These narrow walls can be pinned even at point defects within the crystal (Livingston, 1981).

A fully-saturated magnetization state can be attained by the application of large fields to a crystal of ferromagnetic material. According to micromagnetic theory (Brown, 1963) this state should be very stable. Magnetization reversal in such a state can take place by several modes. The three most commonly suggested modes are (McCaig, 1977, p. 53) (1) rotation of the atomic magnetic moments in unison, (2) buckling, and (3) curling. These latter two modes are incoherent rotation processes. In highly anisotropic materials, such as those commonly used for permanent magnets, theory predicts that reversal should only take place in fields which are much larger (approximately by an order of magnitude) than the highest intrinsic coercivities measured in the laboratory. It is likely that in real materials reversals are nucleated at defects which lower the anisotropy constant in a localized region (Livingston, 1973).

Coercivity Mechanisms in Permanent Magnets

The direction of magnetization in a ferromagnetic material can reverse either by rotation (coherent or incoherent) of the atomic magnetic moments or by the movement of domain walls. In order to obtain high coercivities in permanent magnets, methods must be found to impede: (1) magnetization rotation and (2) the nucleation or growth of reverse domains. These reversal mechanisms have been controlled through various schemes in the manufacture of permanent magnets (Livingston, 1981).

Modern permanent magnet materials can be divided into two classes depending on whether their magnetic anisotropy is shape or crystal based. Elongated single domain (ESD) magnets contain elongated particles of iron or iron-cobalt alloy which have a large shape anisotropy (Luborsky, 1961). The particles are prepared by electrodeposition and are about 10 to 20 nm in diameter. Predictions of high coercivity based on reversal by coherent rotation led to the development of ESD magnets; however, the expected coercivities were never achieved. It appears that reversal in these magnets occurs by a fanning mechanism which is an incoherent rotation process requiring less energy than coherent reversal (Livingston, 1981).

The well-known alnico magnets owe their coercivity at least in part to shape anisotropy. These materials are alloys of aluminum, nickel, cobalt, and iron which transform

into two coherent phases on cooling: a primary ferromagnetic phase and another which is paramagnetic after optimal heat treatment (Livingston, 1981). The phases are aligned, by magnetic annealing, to lie along <100> directions and are about 10 to 50 nm in diameter by 50 to 250 nm long. Reversal is believed to occur by an incoherent rotation process in these materials; however, domain-wall pinning is important in some alnico magnets in which the second phase is weakly ferromagnetic (Livingston, 1981). In this case, particles of the primary phase may be coupled to each other ferromagnetically and the growth of reverse domains is impeded by pinning at fine particles of the second phase (Livingston, 1981).

Barium and strontium ferrites and sintered samarium-cobalt and Nd-Fe-B permanent magnets all have large uniaxial crystal anisotropy (McCaig, 1977, p. 40, and Sagawa and coworkers, 1984a). In these materials, magnetization reversal by coherent or incoherent rotation is very difficult, but measured intrinsic coercivities are always much less than those predicted by a rotation process. It is therefore assumed that reversal occurs by the nucleation and growth of reverse domains (Livingston, 1981).

Nucleation can occur at defects which locally lower the crystal anisotropy. It may also be possible that some reverse domains remain even after magnetizing in a strong field. Pinning sites might lock these domains in place

until a large enough reverse field is applied to break them free. Pinning of domain walls at grain boundaries is known to be important in magnets based on crystal anisotropy, otherwise a single nucleation event could cause the reversal of an entire magnet. Coercivity in two-phase samarium-cobalt magnets is known to be caused by pinning (Becker, 1976).

Coercivity mechanisms in $SmCo_5$ and Nd-Fe-B permanent magnets are discussed in following sections of this chapter.

Magnetization Reversal and Domain Structure: Observational Techniques

Barkhausen (1919) offered the first evidence for the existence of domains by demonstrating that discontinuities (Barkhausen steps) occur during the magnetization of a piece of iron. Bozorth and Dillinger (1931) produced an oscillographic record of a single step in the magnetization curve for a piece of Armco iron and observed many smaller magnetization events. It was concluded that the reversal of one domain causes the change of another domain closely coupled to it magnetically (Bozorth, 1951, p. 531).

Powder Patterns

Magnetic domain structures can be revealed by applying a suspension of magnetite to a polished surface of a ferromagnetic material. Polishing must be done carefully so that the surface is left in an unstrained condition or

domain patterns will be distorted (McCaig, 1977, p. 59). The magnetite particles are attracted to poles which are formed at domain walls. Powder patterns reveal only the surface domain structure which may or may not be representative of that of the bulk material.

Faraday Effect

Domain structure in transparent ferromagnetic materials can be observed by using transmitted polarized light (Dillon, 1963, p. 421). Light passing through the material acquires a rotation in its plane of polarization which depends upon the direction of magnetization within the sample. By rotating an analyzer in the path of the transmitted light, domains can be distinguished as contrasting bright or dark regions. Since the technique is only suitable for transparent materials, the Faraday effect has found its greatest use in studying magnetic bubble memory materials.

Kerr Effect

When plane polarized light is reflected from the surface of a magnetized material a small component of the light has its plane of polarization rotated through a 90^{o} angle (McCaig, 1977, p. 60). This effect can be used to observe domains by use of a metallurgical microscope equipped with a polarizer and analyzer. The net rotation is very small, however, about 5 minutes of arc for iron with

the magnetization parallel to the surface and in the plane of incidence of the polarized light (Dillon, 1963). The effect is strongest for domains with magnetization direction normal to the surface, however only materials with large crystal anisotropy, such as rare-earth-cobalt permanent magnets, can support such domains (McCaig, 1977, p. 60). Usually domains of closure are produced at the surface with magnetization parallel to the surface. For this reason, many recent studies (McCurrie and Mitchell, 1975, den Broeder and Zijlstra, 1975, and Strnat, Li, and Mildrum, 1984) on rare-earth-cobalt magnets have successfully incorporated Kerr-effect analysis.

Transmission Electron Microscopy

When an electron of velocity, $\vec{v}$, passes through a piece of ferromagnetic material it will experience a force which is given by the Lorentz equation:

$$\vec{F} = -e\vec{v}\times\vec{B}, \qquad \text{Eq. 3}$$

where $\vec{B}$ is the local magnetic induction. Electrons will be slightly deflected by this force. However, this effect will not be obvious in the focused image. Instead, out-of-focus images are used to observe the domain structure (Dillon, 1963, p. 424). With special pole pieces, magnetic fields can be applied to the specimen to observe the movement of domain walls. One advantage of this technique over the Kerr effect is that information on magnetization below the

surface of the material is obtained; however, the specimens must be very thin (10 - 100 nm). Another technique, which involves the reflection of electrons from near the surface of a ferromagnetic material, can be used to observe surface domain structure (Mayer, 1957).

Hall Probes

Hall probes can be used to map domain structure in ferromagnetic materials by sensing external fields which result from the magnetization within domains. The Hall effect is the result of the Lorentz force (Eq. 3). As an electric current flows through a conductor in a magnetic field, the charge carriers are accelerated toward one side of the conductor. The simplest arrangement is one in which a current, I, flows through a conductor with a rectangular cross section (see Fig. 5). When placed in a uniform magnetic field, B, directed perpendicular to the conductor (y-direction), a Hall voltage develops across the width of the conductor, the magnitude of which is given by:

$$V = RIBw/A, \qquad \text{Eq. 4}$$

where R is the Hall coefficient, w is the width of the conductor (z-direction), and A is the cross-sectional area of the conductor (Roshon, 1962). Hall coefficients for various materials are given in Table 1. For materials in which conduction by electrons dominates, the Hall coefficient is negative. Hole conduction results in a positive R.

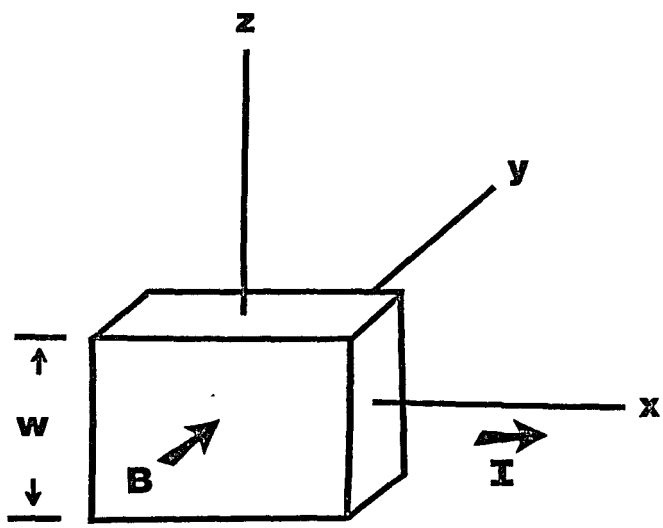

Fig. 5. Hall element.

Table 1. Hall Coefficients of Selected Materials*

Material	Hall coefficient, R ($VmA^{-1}T^{-1}$)	R/ρ ($m^2V^{-1}s^{-1}$)
Ge	-8×10^{-3}	0.14
InSb	-7.5×10^{-4}	7.5
InAs	-7.5×10^{-5}	2.5
Bi	-1×10^{-6}	0.83
Cu	-5.8×10^{-14}	0.035

*Data from Roshon (1962)

In choosing a material for a Hall probe, a high signal-to-noise ratio is most important. This ratio is not related to the Hall coefficient alone but to the ratio of Hall coefficient to resistivity (Roshon, 1962). The materials which are best in this respect are InSb and InAs as shown in Table 1. However, bismuth is sometimes preferred for thin-film probes for domain mapping or sensing because it is easily evaporated. Each component in the compound semi-conductors InSb and InAs has a different evaporation rate making these materials difficult to prepare in thin-film form.

A bismuth Hall probe 12 μm thick with a square sensitive area 20 μm on an edge was used by Kostyshn and coworkers (1960) to map the domain structure in a 200 nm thick cobalt film on a glass substrate. Maps were generated by moving the probe over the film at a distance of about 13 μm. Kerr-effect photographs compared well with maps prepared in this way.

Silicon Hall probes approximately 20 μm in diameter have been made for detecting domains in orthoferrites for magnetic bubble memory devices (Strauss and Smith, 1970). Signals of 0.5 mV were obtained in detecting a single domain.

Rare-Earth Permanent Magnets

Elements with atomic numbers from 58 to 71 are commonly called the rare-earth metals. Scandium, yttrium, and lanthanum are chemically similar to these metals and are sometimes included under the rare-earth classification. The rare-earth elements are distinguished by their electronic structure which is also the source of their unusual magnetic properties. The electron configurations of these elements are given in Table 2 and can be represented by $[Xe]\ 4f^x5d^y6s^2$ where [Xe] is the filled Xe core. Unpaired electrons in the 4f shell are almost entirely responsible for the magnetic behavior of the rare earths (Nesbitt and Wernick, 1973 p. 36), while the outer 5d and 6s electrons are responsible for chemical bonding.

The magnetic moment of an atom is a result of the net angular momentum, J, of its electrons. J is composed of electron spin, S, and orbital, L, angular momenta. When a shell is full, such as the 4f shell in Lu, diamagnetic behavior results since all electrons are paired. In the light rare-earth metals, Ce to Eu, the orbital magnetic moment is larger than that due to spin, however the two contributions are in opposite directions. The magnetic moment of Gd results almost entirely from electron spin; while in the heavier rare earths, the orbital and spin magnetic moments add to produce very large atomic moments at low temperatures (Nesbitt and Wernick, 1973, p. 36).

Table 2. Electron Configurations of Rare Earth Metals

Element	Number of electrons in shell		
	4f	5d	6s
Ce	2	0	2
Pr	3	0	2
Nd	4	0	2
Pm	5	0	2
Sm	6	0	2
Eu	7	0	2
Gd	7	1	2
Tb	9	0	2
Dy	10	0	2
Ho	11	0	2
Er	12	0	2
Tm	13	0	2
Yb	14	0	2
Lu	14	1	2

Interest in ferromagnetic alloys of rare-earth metals came about primarily because of the large magnetic moments in these elements. Naturally, some of the first alloys studied were those with the common ferromagnetic elements Fe, Co, and Ni (3-d transition metals). There is limited solubility in such alloys because of the large atomic sizes of the rare earths compared to the smaller 3-d transition metal atoms. Therefore, intermetallic compounds were of primary interest in the search for materials with unusual magnetic properties.

Nesbitt, Wernick, and Corenzwit (1958) demonstrated that in the Co-Gd and Fe-Gd systems an antiferromagnetic coupling exists between the rare earth and 3-d transition metal atoms. Later, Nesbitt and co-workers (1961) showed that in other RCo_5 compounds (where R is a rare-earth metal) an antiferromagnetic coupling also existed. They also reported the very interesting discovery that although the spin moments in RCo_5 are antiparallel, the orbital moments in the light rare earths (which are larger than and opposite to the spin moments in these elements) would add to the spin moment of cobalt. Thus a large ferromagnetic moment was observed in RCo_5 for R = Y, Pr, Nd, Sm, and Eu while very small moments were found for the heavier rare earths in which spin and orbital moments are parallel (Fig. 6).

Hubbard, Adams, and Gilfrich (1960) made magnetic measurements on $GdCo_5$ and discovered very large intrinsic

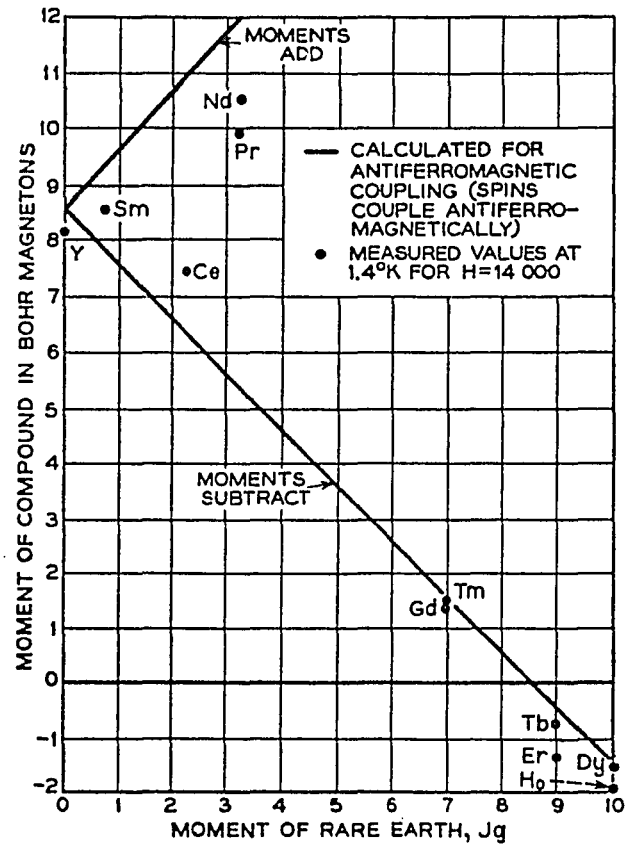

Fig. 6. Variation of magnetic moments of Co_5R compounds with moment of the rare earth element. (From Nesbitt and co-workers 1962).

coercivities for the material in fine powder form. Their results were presumed to be a result of a high magnetocrystalline anisotropy in $GdCo_5$. By magnetic measurements on single crystals, Hoffer and Strnat (1966) found that the hexagonal compound, YCo_5, has a single easy axis of magnetization along the c-axis of the hexagonal cell. A very large anisotropy constant, K_1, of 5.7 MJm^{-3} (see Eq. 2) was determined for this material. The authors stressed the possible importance of YCo_5 as a permanent magnet material. Anisotropy constants and other magnetic properties of some RCo_5 compounds as determined by Strnat and co-workers (1967) are given in Table 3.

Samarium Cobalt Permanent Magnets

Most rare-earth-cobalt permanent magnets are based on $SmCo_5$ because of the high magnetic anisotropy and the ease of making high coercivity materials from this compound (McCaig, 1977, p. 140). Two general types of $SmCo_5$ magnets exist: sintered, primarily single phase magnets, and two-phase magnets containing copper.

Buschow and co-workers (1969) and Das (1969) were the first to announce the preparation of sintered $SmCo_5$ magnets. These magnets had energy products of about 160 KJm^{-3} (20 MGOe) which is considerably larger than had been achieved previously with any other permanent magnet. Minor alloying additions and modifications in processing

Table 3. Magnetic Properties of Some RCo_5 Compounds

Compound	Curie point (^{o}C)	$\mu_0 M_s$ (T)	K_1 (MJm^{-3})
YCo_5	648	1.06	5.5
$LaCo_5$	567	0.909	6.3
$CeCo_5$	374	0.77	5.2 - 6.4
$PrCo_5$	612	1.20	6.9 - 10
$SmCo_5$	724	0.965	8.1 - 11.2

techniques have boosted the maximum energy products of $SmCo_5$ permanent magnets. In one such magnet, prepared from a mixture of $PrCo_5$ and $SmCo_5$, a maximum energy product of 216 KJm^{-3} (26 MGOe) has been achieved (McCaig, 1977, p. 126).

Modern sintered $SmCo_5$ magnets are prepared as follows: (1) cobalt and samarium in the correct proportions are melted together and cast into an ingot (because of the chemical reactivity of rare-earth metals crucible materials must be selected carefully); (2) the ingot is crushed (sometimes in an inert gas or liquid to prevent oxidation of Sm) to a powder with a particle size of about 20 μm; (3) the powder is aligned in a strong magnetic field so that the c-axes (easy magnetic axis) of the individual crystals are parallel; (4) the green compact is then sintered at about 1100°C during which time a liquid phase is produced which aids in densification; (5) finally the sintered magnet is cooled to room temperature and magnetized (Nesbitt and Wernick, 1973, p. 161).

Two-phase samarium-cobalt magnets are prepared by casting a mixture of $SmCo_5$ and $CuCo_5$ (Nesbitt and Wernick, 1973, p. 95). The cast magnets must be subsequently heat treated to precipitate the second phase which brings about high coercivity. One alloy of the composition $Co_{3.5}Fe_{0.5}Cu_{1.35}Sm$ has an intrinsic coercivity of about $3.2x10^5$ Am^{-1} (4000 Oe) in the as-quenched (single phase)

condition which rises to approximately 8.75×10^5 Am^{-1} (11,000 Oe) after aging (Nesbitt and Wernick, 1973, p. 100). These cast two-phase magnets have not found many applications however, because their energy products, approximately 100 KJm^{-3} (12 MGOe), are inferior to the single-phase sintered magnets.

Coercivity Mechanisms in $SmCo_5$ Permanent Magnets

Magnetization reversal in two-phase samarium cobalt magnets is well understood (Becker, 1976). Large coercivities in these materials result from a large crystal anisotropy coupled with the pinning of domain walls at fine (approximately 10 nm) precipitates which are produced during heat treatment. Evidence for this mechanism is found in the magnetic behavior of thermally-demagnetized samples. In the virgin portion of the hysteresis loop (Fig. 7) no appreciable magnetization is induced until a field equal to the intrinsic coercivity is applied. Thus, coercivity is limited by the same source (precipitates) which hinders initial domain wall movement, a conclusion which is supported by Kerr-effect studies (Livingston, 1981). This behavior contrasts with that of sintered single-phase magnets in which virgin magnetization occurs relatively easily (Fig. 7).

Although much is known about coercivity in single-phase sintered $SmCo_5$ magnets, the mechanism by which magnetization reversal takes place is not entirely understood.

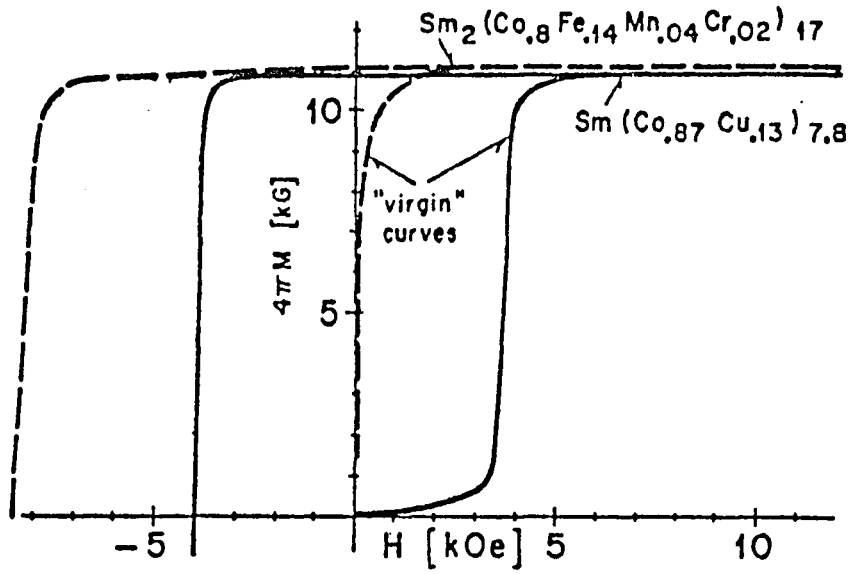

Fig. 7. Magnetization curves for two-phase Sm-Co-Cu and single phase Sm-Co-Fe-Mn-Cr magnets. From Menth and co-workers, 1978).

The new Nd-Fe-B magnets are very similar to these $SmCo_5$ magnets structurally as well as in their magnetic behavior. Consequently the same coercivity mechanism is presumed to control the magnetic behavior of both materials.

Livingston (1973, 1981) has written excellent reviews on coercivity mechanisms in cobalt rare-earths and other materials. Because of the ease of virgin magnetization in sintered $SmCo_5$, large coercivities cannot be the result of uniformly dispersed defects or precipitates as in the two-phase magnets. In fact, TEM micrographs show that the interiors of grains are essentially defect free (Livingston, 1981). It is believed that after complete saturation in a large field, all domain walls are either removed from the magnet entirely or are pushed into sites near the boundaries of grains. Magnetization reversal is then believed to occur when a reverse domain is nucleated at a defect in the grain boundary or by the breaking away of the domain walls which were not completely removed. These persistent domain walls are not easily reversed because of domain-wall surface-tension effects.

Becker (1969) performed some interesting experiments on single crystal particles of $SmCo_5$. By magnetic sieving, he was able to isolate and plot hysteresis loops for a particle of $SmCo_5$ which was about 200 μm in diameter by 500 μm long and other small particles of YCo_5. Because magnetization reversals in these particles occurred in discrete

steps and depended strongly on surface condition, he concluded that nucleation is important in determining coercivity. However he also stated that his results strongly suggest that domain walls are never removed from the particle completely but are only pushed into trapping sites by applying large fields.

Becker (1971) conducted more experiments on small particles of $SmCo_5$ and found that different regions of a single grain particle can act magnetically independently. He concluded that the complex shaped hysteresis loops obtained from some small particles of $SmCo_5$ were really the superposition of loops from different regions of the particle separated by small-angle grain boundaries. Later, Becker (1975) found that multi-grain samples from a sintered $SmCo_5$ magnet behaved similarly to the single grain particles described above. This led to the conclusion that sintered magnets act as a collection of interacting individual particles and that grain-boundary phases which may exist do not influence the behavior of $SmCo_5$ magnets.

den Broeder and Zijlstra (1975) explained the magnetization reversal behavior in sintered $SmCo_5$ magnets as being controlled by both nucleation and pinning of domain walls. The authors divided the demagnetization curve of a typical $SmCo_5$ magnet into two parts with different slope. They theorized that in Part I or low-reverse-field segment, reverse domains were being nucleated while the higher

reverse-field segment, Part II, corresponded to the unpinning of walls of these reverse domains. By subjecting magnets to different heat treatments, the authors were able to control coercivities. These results were correlated, by Kerr effect studies, with an increase or decrease in the number of nucleation sites or with more or less effective pinning at grain boundaries as a result of heat treatment. The authors concluded that nucleation probably occurs at Sm_2Co_{17} precipitates which can form by eutectoid decomposition of $SmCo_5$. Attempts to determine how the pinning effectiveness of grain boundaries could change with heat treatment were inconclusive.

McCurrie (1970) made magnetic measurements on assemblies of particles of $SmCo_5$ and $LaCo_5$. He explained the much higher coercivities measured for $SmCo_5$ as being due to a difference in deformation behavior between $LaCo_5$ and $SmCo_5$ as determined by microhardness measurements. Later McCurrie and Mitchel (1975) studied sintered $SmCo_5$ magnets and concluded that most grains behave as isolated crystals, each with its characteristic nucleation field. Any wall pinning which appeared to have occurred was explained as being internal, that is, occurring within grains rather than at grain boundaries.

Fidler (1981) found that prismatic dislocations in $SmCo_5$ single crystals can act as pinning sites. He also concluded that nucleation of reverse domains occurs at soft

magnetic inclusions. Liu, Strnat, and Mildrum (1982) suggest that reversal in $SmCo_5$ magnets is controlled by pinning at Sm_2Co_7 layers in boundaries between $SmCo_5$ grains. A somewhat paradoxical finding was that reversal became easy above the Curie point of Sm_2Co_7 when pinning should be even more effective. This problem was resolved by theorizing that the soft magnetic behavior of Sm_2Co_7 at high temperatures actually promoted the nucleation of reverse domains.

Strnat, Li, and Mildrum (1984) studied domain patterns in sintered $SmCo_5$ permanent magnets at various stages of magnetization by the Kerr effect. They observed only sudden reversals in individual grains and concluded that isolated nucleation events (occurring at Sm_2Co_7 or Sm_2Co_{17} precipitates at grain boundaries) reported by other investigators have little to do with magnetization reversal in high coercivity $SmCo_5$ magnets. It was presumed that reversal occurs by the unpinning of domain walls from a grain boundary phase. These walls are thought to sweep without impediment through the $SmCo_5$ grains and even across some grain boundaries.

Nd-Fe-B Permanent Magnets

The relative scarcity of Sm and Co resources led to the search for compounds similar to $SmCo_5$ in binary iron-base alloys with the more common light rare earths. Initial attempts at finding such compounds were disappointing

because there are few stable intermetallic phases in LR-Fe systems (LR = light rare earth). Also, those compounds which do form have low Curie points and do not exhibit uniaxial crystal anisotropy (Nesbitt and Wernick, 1973). However the possibility of interesting metastable phases or ternary compounds still remained.

Croat and Herbst (1982) and Croat (1982) prepared non-equilibrium phases in R-Fe alloys (R = Pr, Nd, Sm, Tb, Er) by melt spinning and were able to show that coercivity of each alloy reaches a maximum as a function of quench rate. Later Croat and co-workers (1984) added boron to melt spun Nd-Fe and Pr-Fe alloys with excellent results. Large remanence and coercivity values, which resulted in maximum energy products of about 115 KJm^{-3} (14 MGOe), were obtained at optimum wheel speeds of about 19 ms^{-1}. Koon and Das (1984), Becker (1984), Hadjipanayis, Hazelton and Lawless (1984), and Sellmyer and co-workers (1984) all reported similar results. Post-spinning annealing treatments generally improved permanent magnet properties. Consequently the above investigators were led to believe that the phase which was responsible for the large measured coercivities was actually an equilibrium compound.

Sagawa and co-workers (1984a) were the first to produce a permanent magnet based on the new compound, which was identified by Croat and co-workers (1984) as $Nd_2Fe_{14}B$. Their magnet was made by the same powder metallurgy

techniques developed for $SmCo_5$ sintered magnets except that a post-sintering heat treatment at about 600°C was required to bring about maximum coercivity. The optimum composition for these magnets was found to be near $Nd_{15}B_8Fe_{77}$. This composition was shown to result in magnets containing mainly three phases (Sagawa and co-workers 1984b): the $Nd_2Fe_{14}B$ matrix phase (or hard compound), a Nd-rich phase consisting of 95 at.% Nd, 3-5 at.% Fe and a trace of B, and a B-rich phase of approximate composition $Nd_2Fe_7B_6$.

A photomicrograph of a typical magnet microstructure is shown in Fig. 8. The Nd-rich phase surrounds the grains of $Nd_2Fe_{14}B$ while the B-rich phase is present in only very small amounts. Sagawa and co-workers (1984b) identified the low-melting Nd-rich phase as being a sintering aid, leading to rapid densification of the magnet and bringing about high coercivities. The increase in coercivity was presumed to be a consequence of this Nd-rich phase becoming liquid during sintering and etching damaged surfaces of $Nd_2Fe_{14}B$ grains. Stadelmaier and co-workers (1984) believed the increased coercivity to result solely from a decrease in particle size of the hard compound.

The crystal structure of $Nd_2Fe_{14}B$ was determined by Herbst and co-workers (1984) and by Shoemaker, Shoemaker, and Fruchart (1984). The tetragonal unit cell (Fig. 9) contains four $Nd_2Fe_{14}B$ units or 68 atoms in all. Herbst and co-workers also determined that all Nd and Fe magnetic

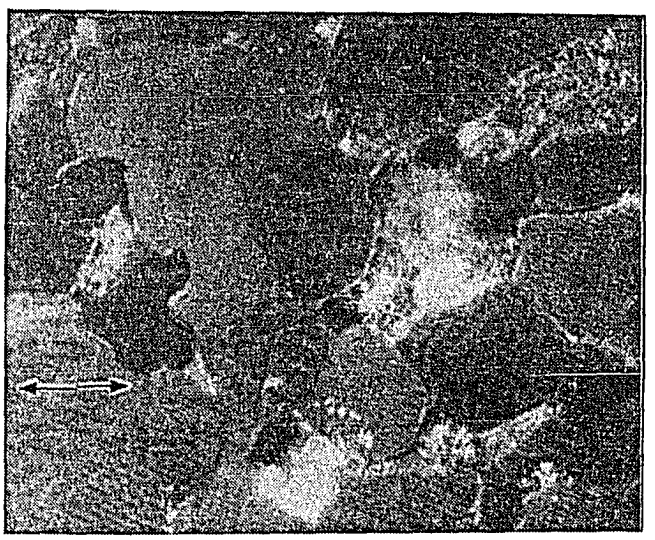

Fig. 8. Microstructure of a typical Nd-Fe-B magnet. Arrows indicate 10 μm. (From Livingston, 1985).

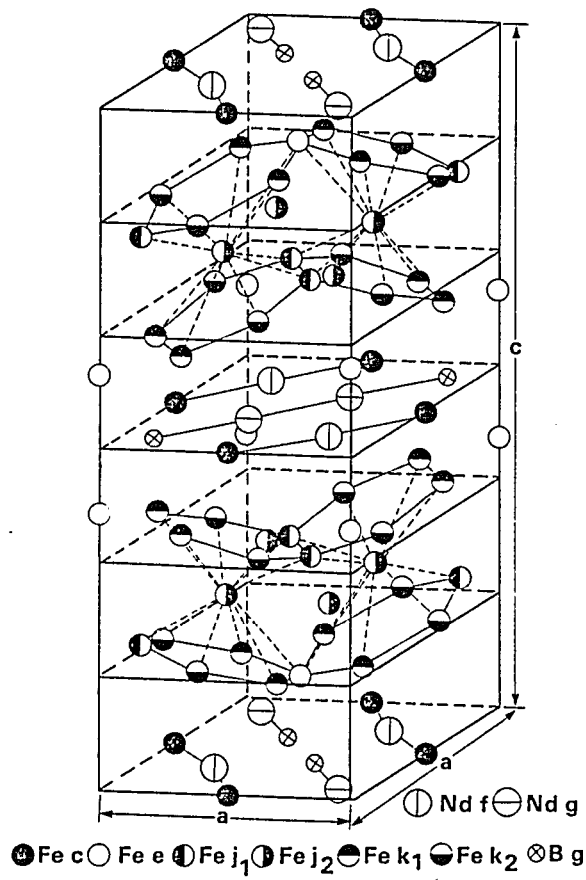

Fig. 9. Unit cell of $Nd_2Fe_{14}B$. From Herbst and co-workers, 1984).

moments lie parallel to the c-axis of the tetragonal cell which verified that the moments are coupled ferromagnetically.

Coercivity Mechanisms in Nd-Fe-B Permanent Magnets

As stated earlier, the microstructure and magnetization characteristics of the new Nd-Fe-B and sintered $SmCo_5$ magnets are very similar. Therefore it is likely that the coercivity mechanism in both materials is the same and many of the theories proposed for magnetization reversal in $SmCo_5$ have been carried over to explain behavior in Nd-Fe-B. Perhaps the most interesting magnetization behavior in both magnets is the dependence of B_r and H_{ci} on the strength of the maximum magnetizing field (Fig. 10). Sagawa and co-workers (1984a) explain this phenomenon in terms of local pinning zones within each grain which trap domain walls at different depths. This explanation was challenged by Handstein and co-workers (1985) who believe that the magnetization behavior in Nd-Fe-B can be explained entirely on the basis of a nucleation model.

Livingston (1985) studied domain structures in Nd-Fe-B magnets using the Kerr effect and observed the following: (1) as in $SmCo_5$ magnets domain walls are not strongly pinned within grains and (2) grains in field-demagnetized specimens are mostly multidomain. Statement (2) contrasts observations in $SmCo_5$ in which most grains

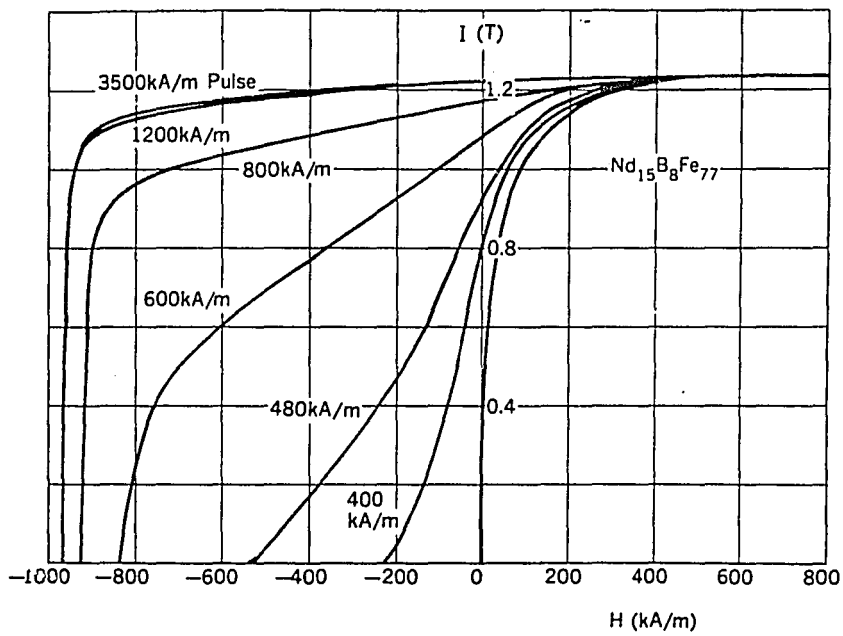

Fig. 10. Magnetization curves for a typical Nd-Fe-B magnet. (From Sagawa and co-workers, 1984a).

are single domain in the field-demagnetized state. This discrepancy was believed to be the result of the much lower coercivity in the Nd-Fe-B sample studied compared with that of $SmCo_5$ magnets.

Li and Strnat (1985) also studied domain patterns in Nd-Fe-B permanent magnets by the Kerr effect. Domain walls were found to move easily within grains but pinning was found to occur along grain boundaries. Upon lowering fields from a large forward value, spike-shaped reverse domains appeared, mostly at grain boundaries. By further lowering the applied field, the spike domains grew reversibly. These domains could be made to disappear by reversing the field, and reappear at the same location by reapplying the field. This process occurred smoothly unless the "suppression field" was too large, in which case the spikes "popped" into place irreversibly. Based on these observations it was concluded that reversal within individual grains does not occur by nucleation of a reversed domain but by the expansion of residual reversed domains from pinning sites at grain boundaries.

By Kerr effect and Bitter technique studies, Tiesong and co-workers (1986) confirmed the results of Livingston (1985) and Li annd Strnat (1985). They also made the very interesting discovery that some reverse domains can extend even across grain boundaries. This observation is consistent with TEM domain observations made by Suzuki and

Hiraga (1986) which show that domain walls can exist within the grain boundary region (presumably within the intergranular Nd-rich phase).

Hadjipanayis, Lawless, and Dickerson (1985) recorded Barkhausen steps in a magnetic viscosity curve for a sample of a Nd-Fe-B magnet at 10 K. These steps were attributed to domain walls becoming pinned and unpinned at grain boundaries. The authors reported that each step corresponded to the magnetic reversal of a volume of material close to the volume of a single grain but did not say how this was determined.

Grain boundaries in Nd-Fe-B permanent magnets were observed by Hiraga and co-workers (1985) using high-resolution electron microscopy. They found that most $Nd_2Fe_{14}B$ grains were joined by a new bcc phase and observed that the microstructure at these boundaries changed significantly with heat treatment. After heat treatment for maximum magnet coercivity, the boundary appeared smooth. However, in a low-coercivity magnet, platelets of this bcc boundary phase extended into the $Nd_2Fe_{14}B$ grains, presumably becoming sources for the nucleation of reverse domains. Fidler (1985) also observed a grain boundary phase by high-resolution electron microscopy but instead concluded that the soft magnetic boride phase, $Nd_2Fe_7B_6$, (also reported by other investigators) controlled the coercivity

of Nd-Fe-B magnets by acting as nucleation sites for reverse domains.

CHAPTER 3

OBJECTIVE

The purpose of this investigation was to use a Hall-effect microprobe to study domain wall motion in a sample of neodymium-iron-boron permanent magnet material. Information obtained from this study is intended as a supplement to domain observations of other investigations utilizing the Kerr effect and Lorentz electron microscopy, techniques which are severely limited in regard to information about bulk domain processes. It is hoped that the qualitative and quantitative information obtained herein will provide a better understanding of the nature and importance of domain wall pinning at grain boundaries in Nd-Fe-B and will shed some light on the processes of local magnetization reversal in this material.

CHAPTER 4

EXPERIMENTAL PROCEDURE

Domain wall motion in the Nd-Fe-B magnet sample was sensed by measuring voltage changes in a Hall microprobe which was placed on a polished surface of the sample. Magnetization changes (domain wall motion) in the magnet sample were induced by placing the probe-sample assembly into an electromagnet, and by gradually increasing or decreasing the field. Details of the equipment used for the above measurements and experimental procedure are given in the following sections.

Permanent Magnet Sample

The permanent magnet used for this study was a NEOMAX-35 magnet obtained from Magnet Sales and Manufacturing Company of Culver City, California. The magnet was produced by the Sumitomo Special Metals Company of Japan by the general method described in an early paper (Sagawa and co-workers, 1984a). The procedure is as follows:

(1) Neodymium, iron, and boron are induction melted in the atomic proportions 15:77:8 in an alumina crucible under an argon gas atmosphere and cast.

(2) Ingots are crushed, pulverized, and milled in a protective atmosphere to a particle size of about 3 μm.

(3) The powder is aligned and compacted in a strong magnetic field and sintered in argon for 1 hr. at about 1000°C.

(4) Finally the sintered compacts are given a post-sintering heat treatment at about 600°C to bring about high coercivity.

A photomicrograph of a polished surface of the magnet used in this investigation is shown in Fig. 11. The magnet consists of grains of $Nd_2Fe_{14}B$ surrounded by a Nd-rich grain boundary phase (which is removed by the etchant). The average $Nd_2Fe_{14}B$ particle size for this particular magnet is about 10 μm larger than the 3 μm quoted in early papers from the Sumitomo group.

Electromagnet and Related Circuits

The electromagnet used in this investigation was constructed from the laminated core of a neon-sign transformer (Fig. 12). The core was cut and fitted with two conical pole pieces, each having an included angle of 60°, which were machined from hot-rolled steel. Two thousand turns of 18-gauge copper magnet wire comprised the windings of the electromagnet which were divided into 10 packs of 200 turns each. These packs were connected in parallel, giving a total resistance of about 0.1 Ω.

Since a stable magnet current is essential for the type of Hall-probe measurements made in this study, a

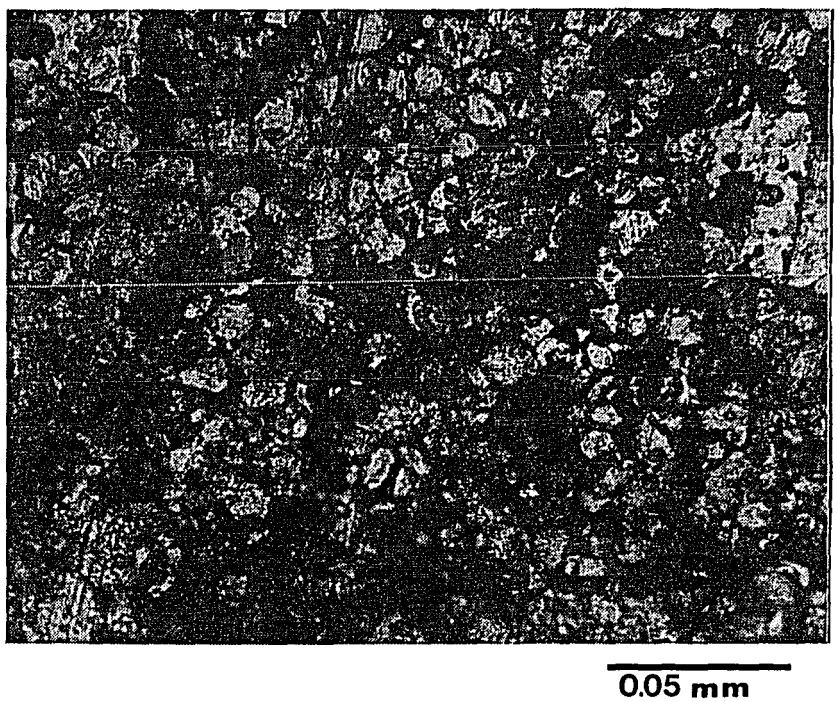

Fig. 11. Photomicrograph of a polished surface of the Nd-Fe-B magnet used in this investigation.

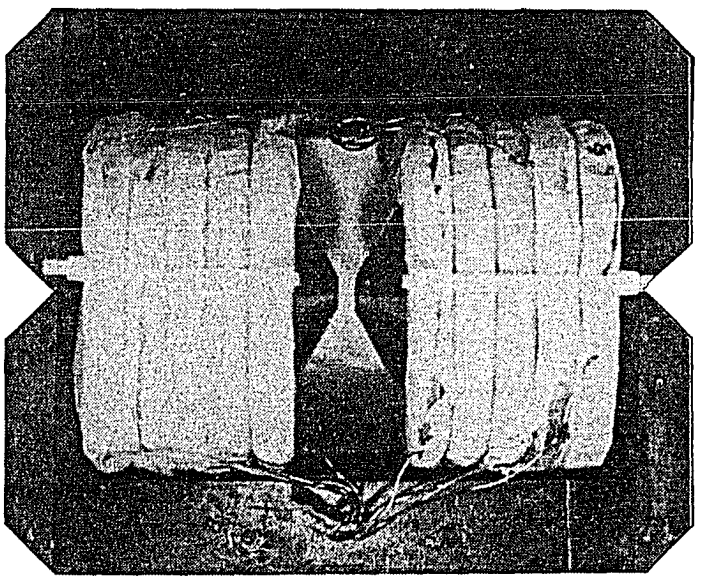

Fig. 12. Electromagnet made from the core of a neon-sign transformer. (Approximately one-half actual size).

12-volt automobile battery was used as a power source, instead of a rectified alternating current source. An 8-ampere recharger was used to charge the battery between tests. Current to the electromagnet was regulated with a thermistor in series with the electromagnet windings.

Thermistor Control

The thermistor was constructed from a disk, approximately 1 mm thick by 7 mm in diameter, of high purity silicon with a room temperature resistivity of 5.8×10^4 Ωcm. A layer of platinum silicide was formed on the surface of the silicon disk by dipping the disk in a solution of $H_2PtCl_6\cdot6H_20$ in ethanol, followed by heating the disk in a furnace at 900°C for a few minutes. This process was repeated several times until a continuous metallic looking surface was obtained. After removing the platinum silicide layer from the rim of the disk by grinding, the disk was clamped between two cylindrical blocks of graphite. The graphite blocks in turn contacted silver strips which served as electrical leads to the device (Fig. 13).

By heating the carbon blocks of the thermistor to about 300°C through an external nichrome coil, the resistance could be smoothly reduced from a room temperature value of 37 KΩ to less than 0.1 Ω. A smooth variation over such a wide range is difficult to obtain with any other type of resistor, especially when the high currents which are

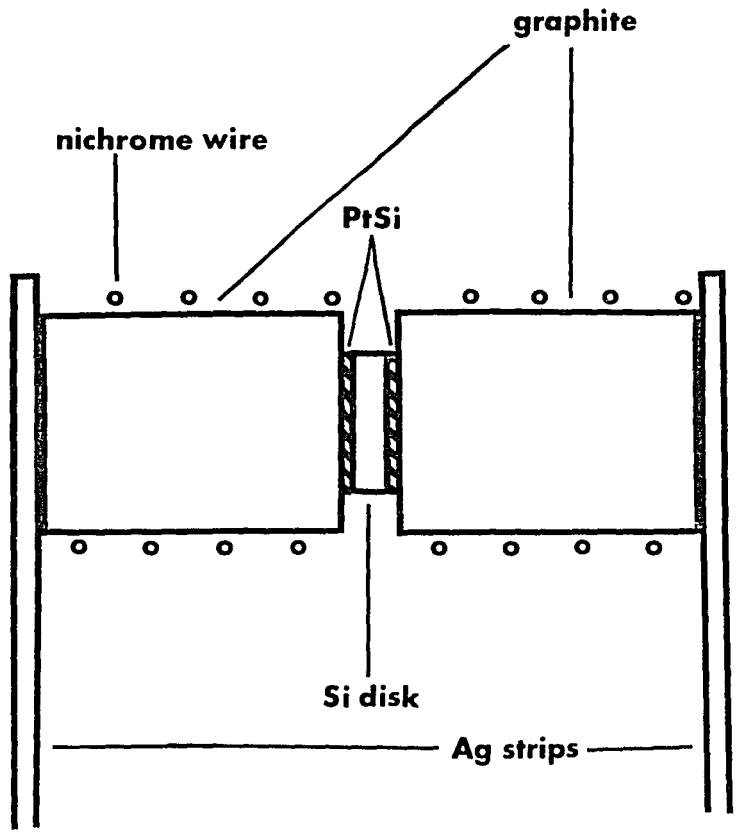

Fig. 13. Schematic diagram of the thermistor which was used to control the current to the electromagnet.

required for the electromagnet are considered. One disadvantage of the thermistor, as described below, is thermal runaway.

Thermal runaway occurs when the current passing through the thermistor becomes large enough to increase the temperature of the silicon disk. The result is a continuous decrease in resistance and a corresponding increase in current until the current is limited by other resistances in the circuit. Thus, in order to reduce the current to the electromagnet once runaway had occurred, a modification which allowed the thermistor to be force cooled was made. Cooling was achieved by replacing the leads to the thermistor with hollow-channel brass strips through which water could be circulated. In practice, reducing the current through the thermistor was possible with the modification, however precise control was difficult.

Magnetic Field Measurement

The entire electromagnet circuit is shown in Fig. 14. Magnetic fields were measured with a ballistic galvanometer whose deflection is proportional to the flux change through a coil inserted into the field and connected to the galvanometer. The relationship is given by the following equation:

$$D = K\int Edt = K\Delta\phi = KNA\Delta B, \qquad \text{Eq. 5}$$

where D is the maximum deflection of the galvanometer, E is

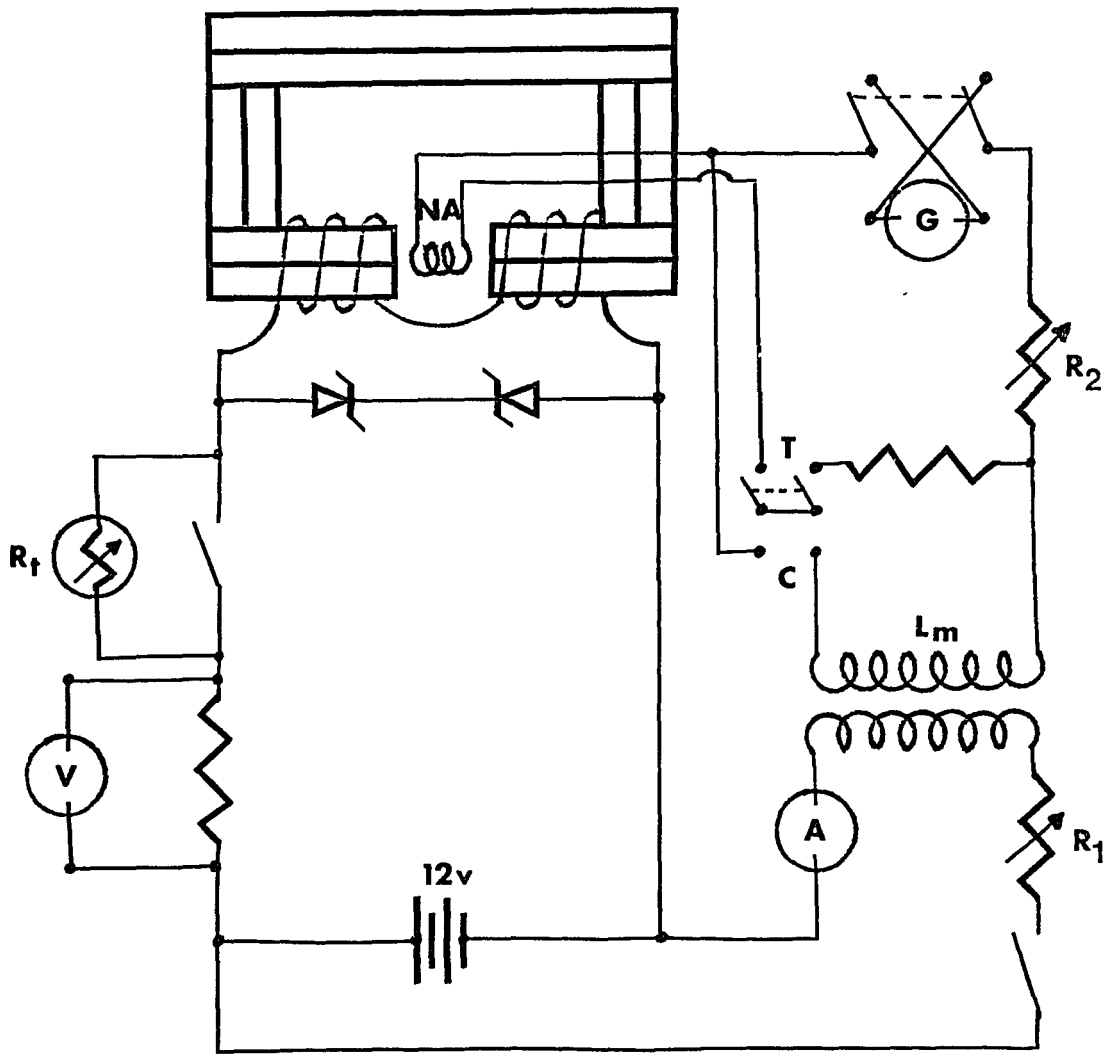

Fig. 14. Electromagnet circuit. (G) galvanometer for measuring magnetic fields, (A) ammeter and (L_m) mutual inductor for calibration of the galvanometer, (R_2) calibration resistor, (NA) field sensing coil, (R_T) thermistor, (V) voltmeter for determining electromagnet current. The two Zener diodes have breakdown voltages of 14 V. (R_1) is used for determining the galvanometer deflection--field relationship.

the instantaneous voltage produced by the coil during the flux change, $\Delta\phi$ is the magnetic flux change, N and A are the number of turns and area of the coil, and ΔB is the change in magnetic induction or field. The constant K is determined through calibration of the galvanometer as described below.

Calibration of the galvanometer was achieved by the use of a mutual inductor. If the mutual inductance, L_m, between two coils is known, the magnetic flux, ϕ, through one coil due to a current in the other I_2, is given by:

$$\phi_1 = L_m I_2. \qquad \text{Eq. 6}$$

By switching I_2 on or off, a known flux could be made to pass through Coil 1. Connecting Coil 1 to the galvanometer and measuring the deflection when the current is turned on or off allowed the constant K in Eq. 5 to be determined.

A mutual inductor was made by winding 265 turns of 22-gauge copper magnet wire over 1170 turns of 36-gauge wire on an 8 cm diameter spool 19.6 cm long. The solenoidal shape of the coils allowed the mutual inductance to be easily calculated using

$$L_m = \mu_0 N_1 N_2 A/\ell, \qquad \text{Eq. 7}$$

where μ_0 is the permeability of free space, N_1 and N_2 are the numbers of turns in the two coils, A is the cross-sectional area of the spool, and ℓ is the length of the coil pair. In this way L_m was calculated to be 10 mH for the inductor.

In order to check the validity of the above calculations, the mutual inductance of the coil pair was measured by a simple technique. A triangular wave signal was fed into the 36-gauge coil and the voltage output from the second coil was measured on an oscilloscope. Knowing the slope of the voltage input signal, dV_1/dt, the resistance of the input circuit R, and the output voltage V_2, the mutual inductance can be calculated using:

$$V_2 = (L_m/R)\ dV_1/dt. \qquad \text{Eq. 8}$$

By this technique L_m was measured to be 9.7 mH, comparing well with the value of 10 mH calculated above.

The galvanometer deflection was found to have a linear relation with calibration current in the mutual inductor (Fig. 15). By adjusting the calibration resistor (Fig. 14), the deflection could be made to correspond to some convenient multiple of the measured field (Eq. 5). Once calibrated, the galvanometer was used to correlate the field produced in the gap of the electromagnet with the current to the electromagnet. The relationship is shown in Fig. 16 where the field is plotted against the voltage across a resistor in series with the electromagnet. This voltage, which is proportional to the electromagnet current, was used as a measure of the field in all subsequent experiments.

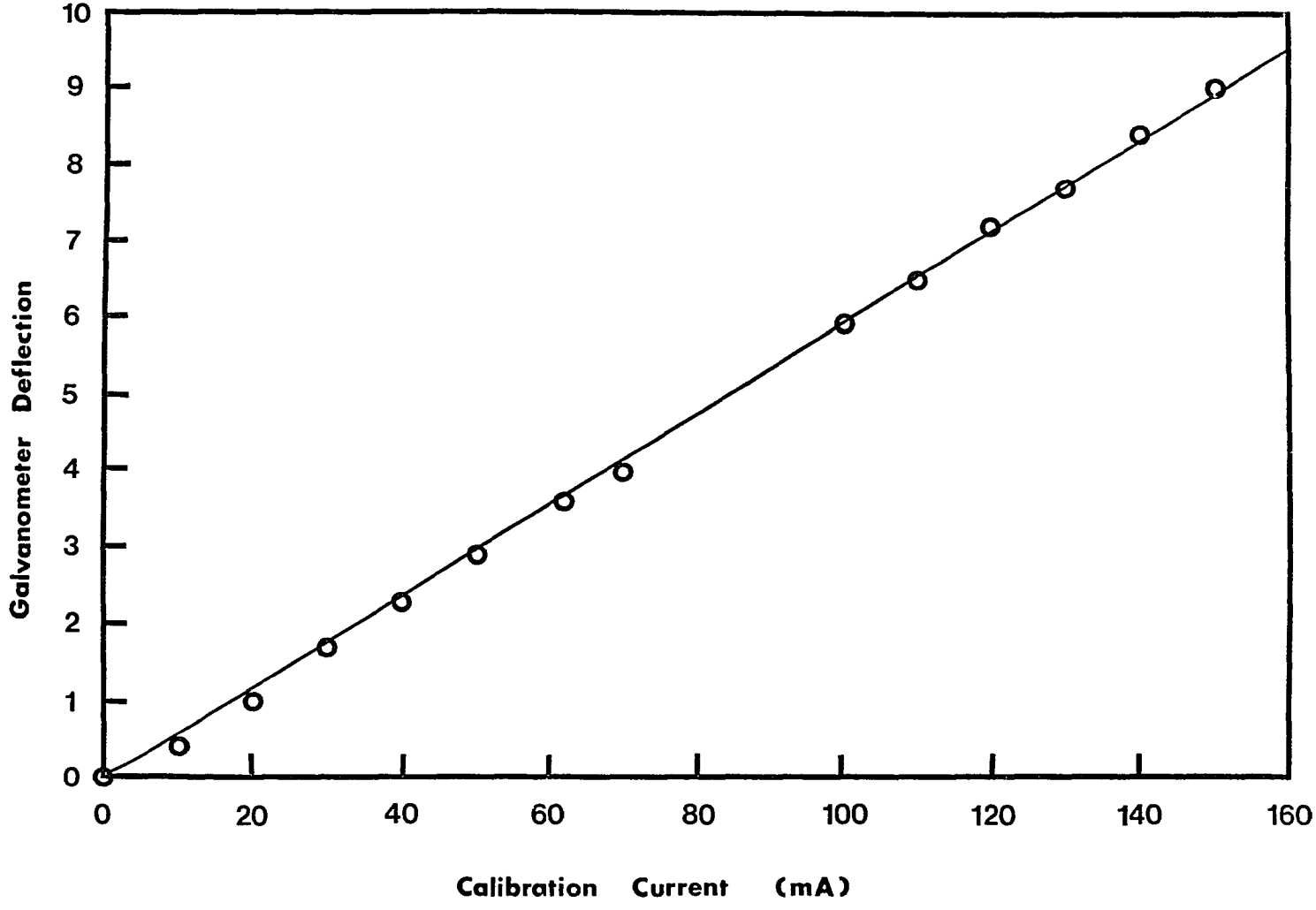

Fig. 15. Galvanometer deflection versus current change in the primary coil of the mutual inductor.

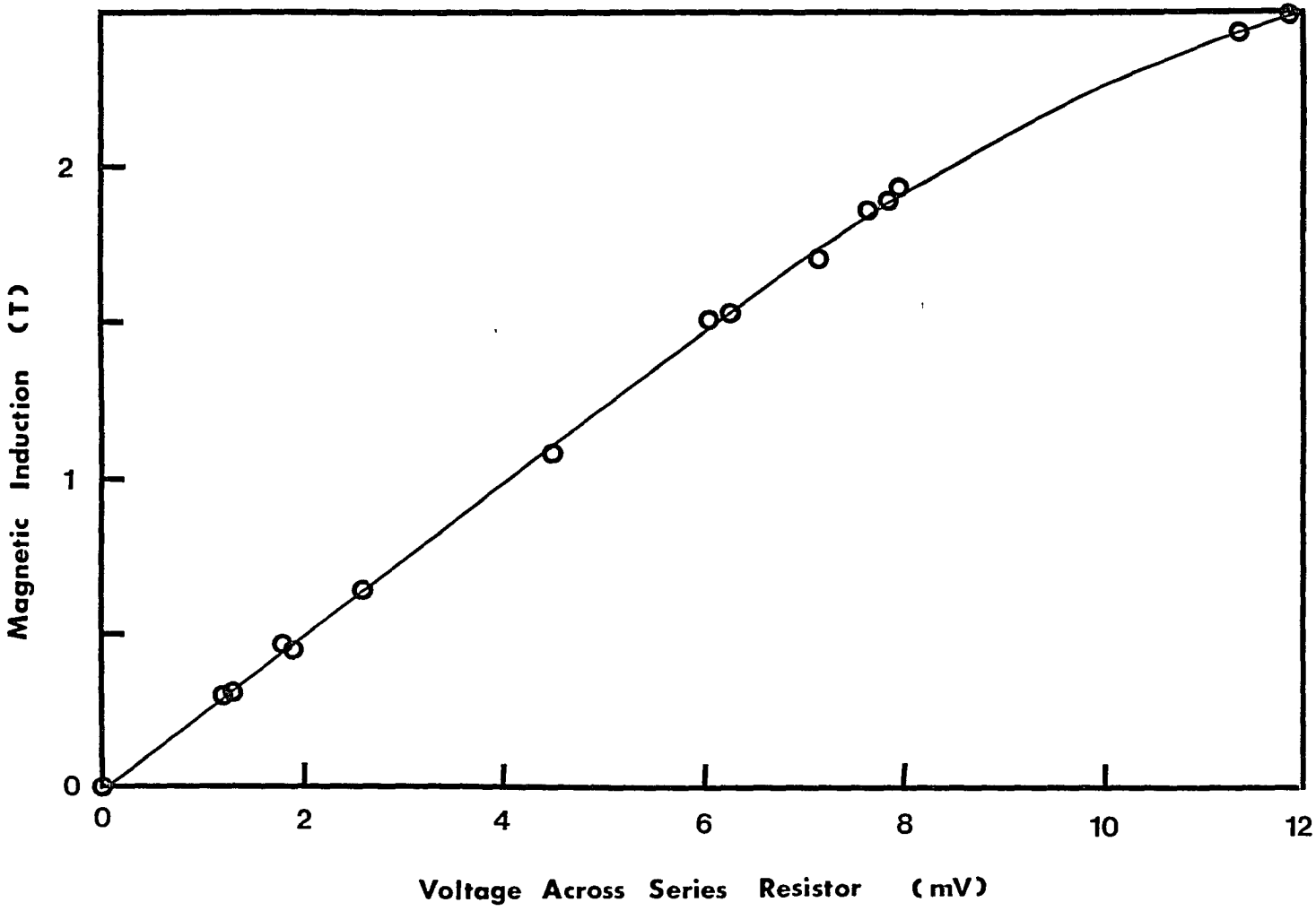

Fig. 16. Magnetic induction in the gap of the electromagnet versus the voltage across a series resistor in the electromagnet circuit.

Hall Probes

Hall-effect microprobes were prepared by evaporating, in a vacuum chamber at about 10^{-4} torr, thin films of bismuth through a stencil mask onto glass microscope slides. Bismuth was evaporated from a molybdenum boat which was resistance heated to about 600°C. The masked glass slides were placed 10 cm above the bismuth source where the deposition rate was about 0.5 nms^{-1}.

Masks

The primary masks, which were used for defining the Hall element, were made from a silicon wafer used in the electronics industry. This wafer was 500 μm thick and had been sawn three quarters of the way through one face with a 75 μm-wide blade for dicing. Pieces of the wafer which consisted of four adjacent dice (with grooves forming a cross between dice) were mounted in a low melting point wax onto the pedestal of a dimpling machine used for TEM sample preparation. A dimple was ground into the reverse side of each four-die piece, exposing a cross pattern and forming the Hall-element mask (Fig. 17).

Hall-element masks were attached with 1/64-inch-wide drafting tape to half-inch-wide glass microscope slides. The glass slides were pre-cleaned in a 4-step process which consisted of: (1) soaking in concentrated nitric acid, (2) rinsing in distilled water, (3) rinsing in acetone, and

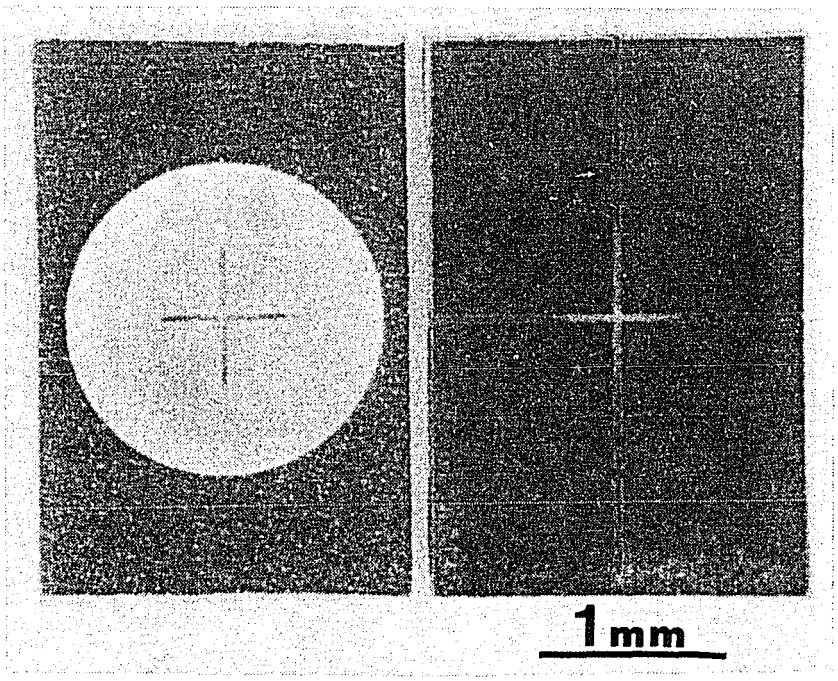

Fig. 17. Pieces of a silicon wafer used as a mask for preparation of thin-film Hall probes. The "+" pattern, which was formed by grinding a dimple into the reverse side of a pre-sawn wafer, was formed by the intersection of two 75 μm-wide grooves.

(4) plasma etching for 60 s in argon. Aluminum foil was used to cover the unmasked areas of the slide during the primary evaporation to form the Hall-element.

A second evaporation of bismuth was required to form leads to the Hall element. This time drafting tape was used to mask the active area of the element and to form a lead pattern. The probe preparation process is summarized in Fig. 18. In each evaporation step approximately 10 μm of bismuth was deposited. Finished probes (Fig. 19) were coated with a layer of lacquer for electrical insulation and to protect the active area from mechanical damage.

Forty-gauge copper wire was used to make electrical connection to the probes. The wires were attached with small chunks of indium metal which stuck well to the bismuth film when pressed with a small tool. The optimum probe current was in the neighborhood of 10 mA. This produced a large Hall voltage for a given magnetic field without excessive heating of the Hall element. A 12 V battery was used as a power supply.

Electrical Characteristics of the Probes

Hall voltage versus applied magnetic field for one of the probes is shown in Fig. 20. The probe current in this case was 10 mA. In all probes a non-zero voltage was present even when no magnetic field was applied. This effect is probably due to asymmetry of the Hall element.

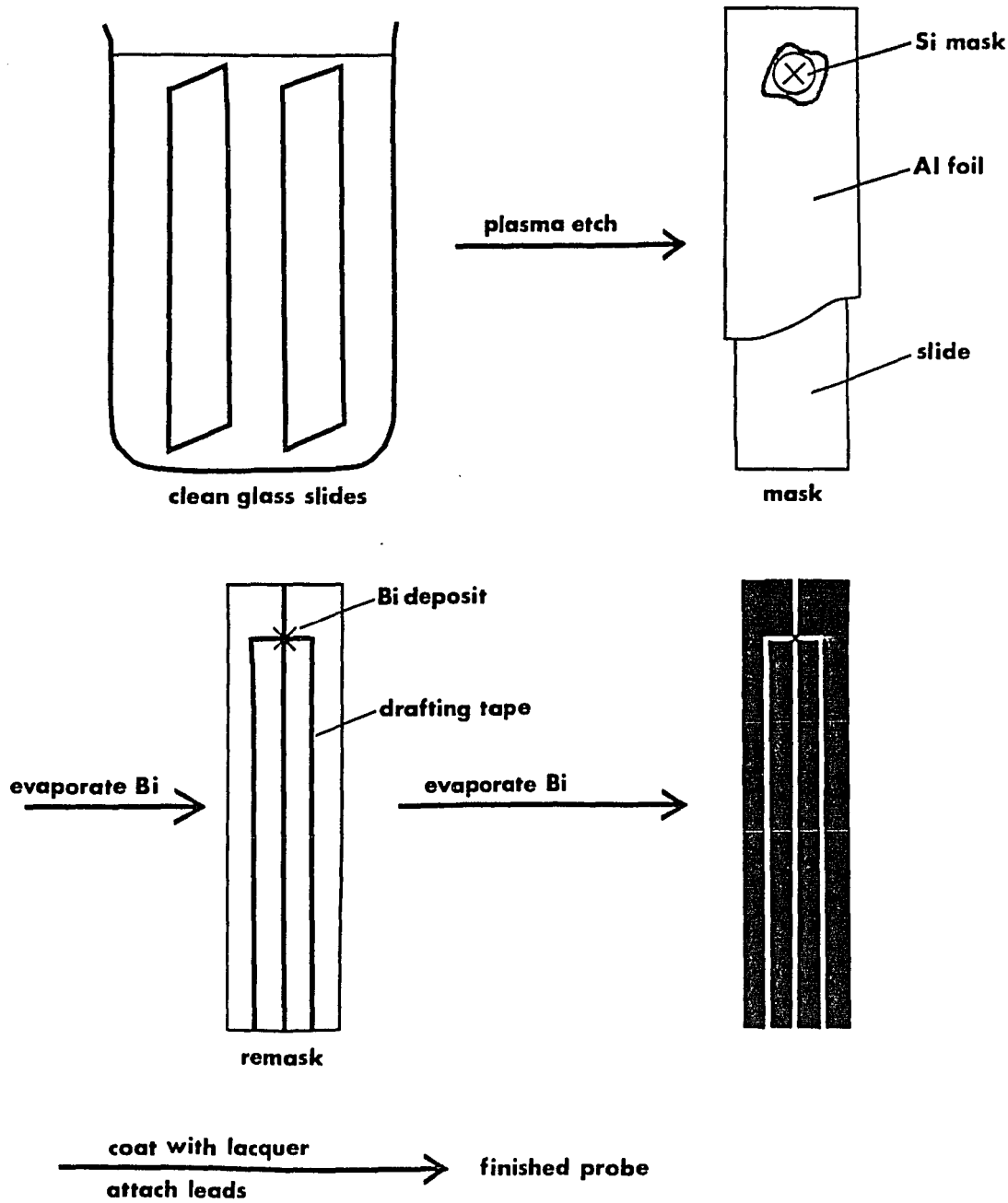

Fig. 18. Preparation of Hall microprobes by vacuum deposition of bismuth onto masked microscope slides.

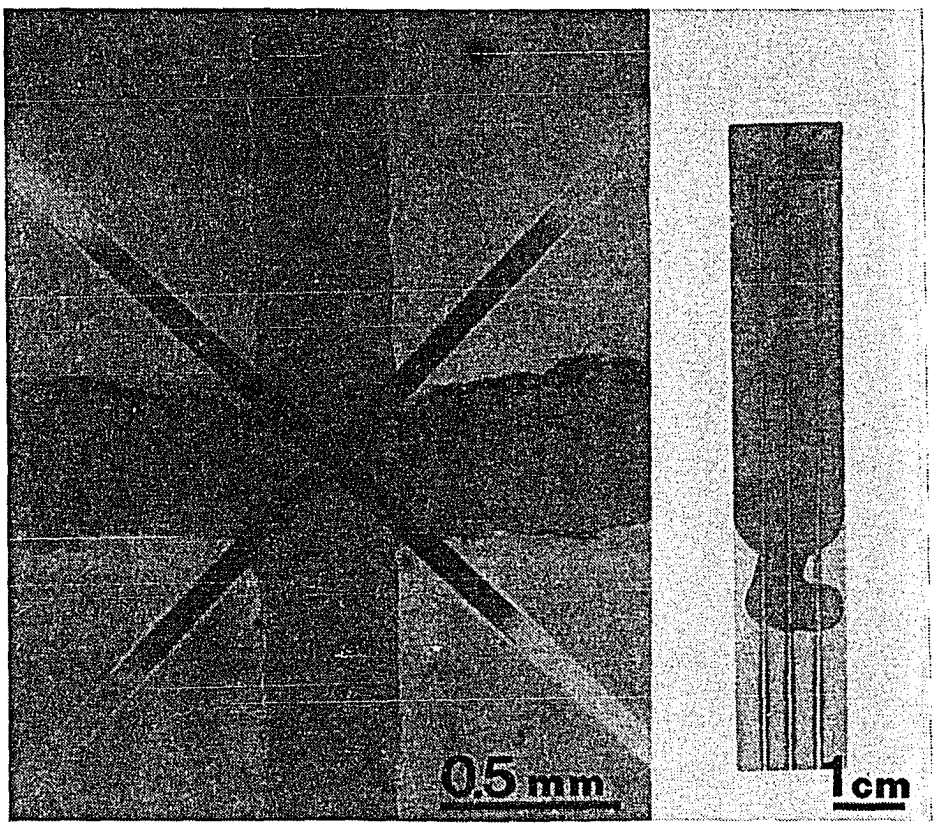

Fig. 19. Hall probe, high and low magnification.

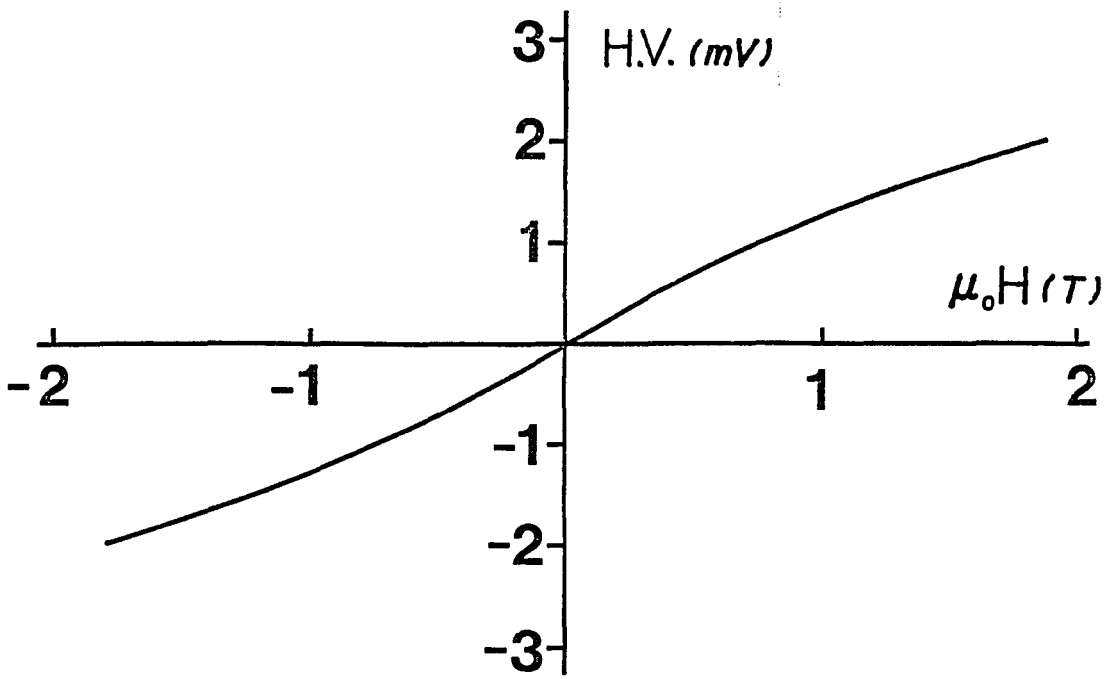

Fig. 20. Characteristics of the blank probe for a probe current of 10 mA.

In order to make a zero Hall voltage correspond to zero applied field, the offset voltage had to be subtracted from each voltage reading.

Specimen Preparation

Specimens were in the form of plates (approximately 5 mm square by 0.5 mm thick) prepared from chips from the fully magnetized NEOMAX-35 magnet. Each chip was oriented in the field of a permanent magnet, embedded in a low-melting wax, and polished flat. The polished surface in each case was perpendicular to the axis of easy maganetization. Each piece was then removed from the wax and mounted in casting resin so that the opposite face could be polished flat. Measurements were made on this second face with the specimen in the mount. A second set of specimens was prepared in the same way except that the magnet chips were thermally demagnetized by heating in an evacuated quartz tube (gettered with Nd powder) to about 400^{o}C for a few minutes and cooling before mounting in resin.

Testing Procedure

Domain wall motion was sensed by placing a Hall probe face down onto a plate of magnet material in the casting-resin mount and fixing the probe in place with plastic tape. This assembly was then inserted into the electromagnet so that the Hall element was centered on the axis of the pole pieces.

The basic structure of all experiments involved recording, on an x-y recorder, the Hall voltage of the probe while changing the applied field. Experiments were divided into three classes: (I) field demagnetization of fully magnetized samples, (II) cyclic magnetization of initially demagnetized specimens in fields of increasing amplitude, and (III) cyclic magnetization of initially demagnetized specimens in fields of constant amplitude. These experiments are described below.

I. Field Demagnetization of Fully Magnetized Samples

These experiments consisted of applying a slowly-increasing reverse field to a sample of the fully magnetized Nd-Fe-B magnet while recording the Hall voltage of a probe fixed to the sample surface.

II. Cyclic Magnetization of Initially Demagnetized Specimens in Fields of Increasing Amplitude

These experiments consisted of placing a Hall microprobe on the surface of a thermally demagnetized sample of the Nd-Fe-B magnet. The Hall voltage of this probe was recorded during the following procedure:

(1) initial magnetization in a weak field by slowly increasing the applied field from 0 T to about 0.25 T,

(2) initial demagnetization by slowly decreasing the applied field to approximately -0.5 T,

(3) remagnetization by again increasing the applied

field--this time to a value of 0.75 T,

followed by subsequent demagnetizations and remagnetizations in fields of higher and higher amplitude until the limit of the electromagnet system, 2 T, was reached.

III. Cyclic Magnetization of Initially Demagnetized Specimens in Fields of Constant Amplitude

These experiments are the same as Type II except that on each cycle of magnetization the applied field was slowly increased or decreased to a constant amplitude of about 2 T.

CHAPTER 5

RESULTS AND DISCUSSION

The experimental arrangement described in the previous chapter allows for the detection of magnetization changes in very small volumes of the permanent magnet material. The principle is as follows. The Hall microprobe produces a voltage which is proportional to the magnetic field within the active volume of the probe. This field has two sources: the applied field, H, and the magnetization within the sample, M. These two fields combine to produce a net field in the vicinity of the probe (Fig. 21). In principle, the magnetization of the sample could be determined for any applied field from the measured Hall voltage. In the simple case in which the fields from the magnetization of the sample and electromagnet are assumed to be uniform and perpendicular to the probe surface (this would be the case for an infinitesimal probe located directly above a single domain), the magnetization is given by:

$$M = H(V)-H, \qquad \text{Eq. 9}$$

where H is the applied field and H(V) is the field which corresponds to the measured Hall voltage. In practice Eq. 9 is not applicable because the domain structure near the surface of the sample will not in general produce a

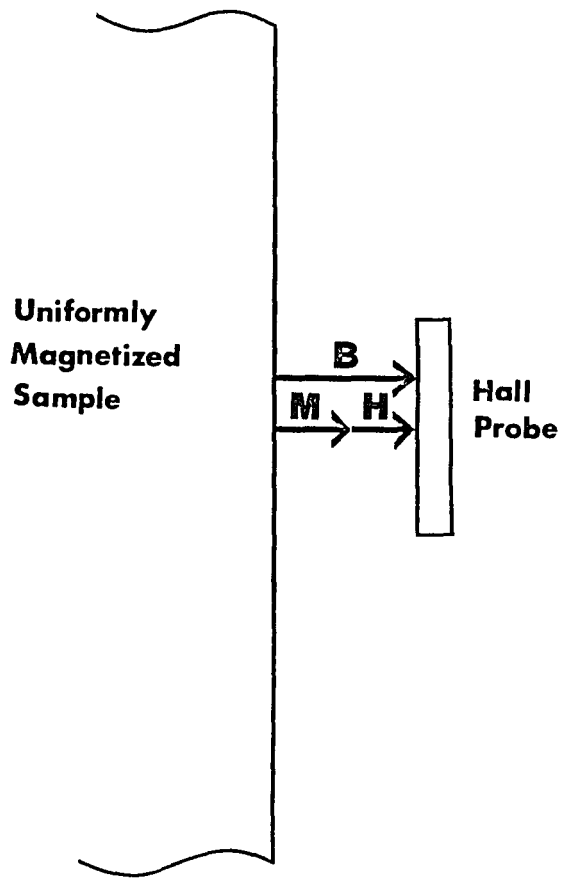

Fig. 21. Magnetic field sensed by the Hall probe near a uniformly magnetized sample. The Hall probe senses the combination, B, of the magnetization of the sample, M, and the applied field, H. For this simple configuration M can be determined from M = H(V)-H where H(V) is the field which corresponds to the measured Hall voltage and H is the applied field.

uniform field in the active volume of the probe. Thus quantitative determination of M is not possible. Instead, the traces of probe voltage versus applied field (given below) are valuable mostly for qualitative information regarding magnetization changes and domain wall movement within the permanent magnet material. It will be shown that much can be learned from this information.

Demagnetization of Fully Magnetized Samples

A typical Hall voltage trace (from an x-y recorder) for the demagnetization of a fully magnetized sample is shown in Fig. 22. In this, as in all traces, the applied field was increased and decreased at a rate of about 50 mTs^{-1}. The steps which occur in the trace are the result of rapid domain wall motion and are known as Barkhausen steps. On studying Fig. 22, it can be seen that the Barkhausen steps can be either positive--adding to the voltage produced by the applied field; or negative--subtracting from the voltage. This phenomenon occurs because the sample extends beyond the active area of the probe. The magnetization from a volume of material adjacent to the active probe area produces a field in the active area which is opposite to that produced if the same volume of material were located directly under the probe (Fig. 23). At first this appears to be a disadvantage of the technique, but actually it allows distinction to be made between

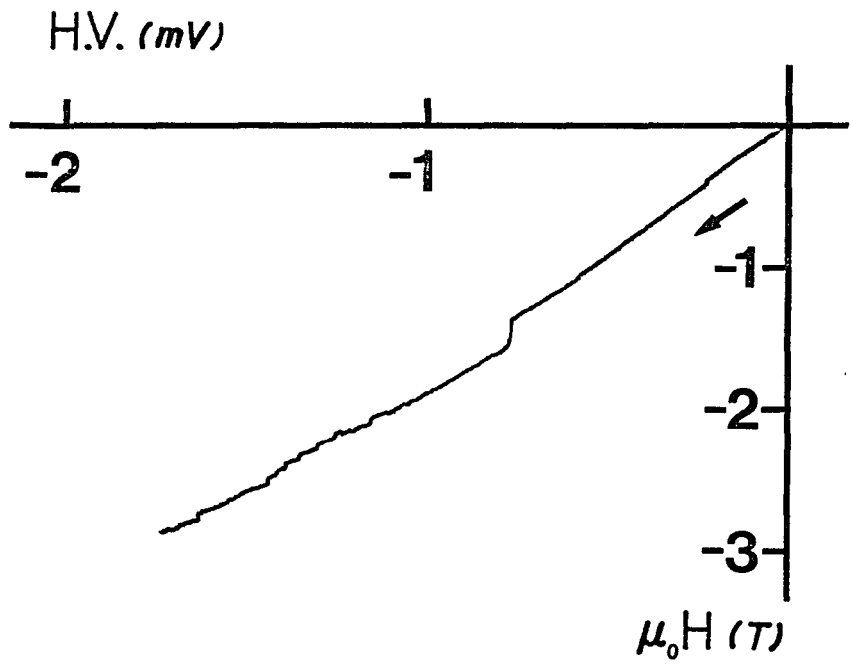

Fig. 22. Hall voltage trace for the demagnetization of a fully magnetized sample of the Nd-Fe-B magnet.

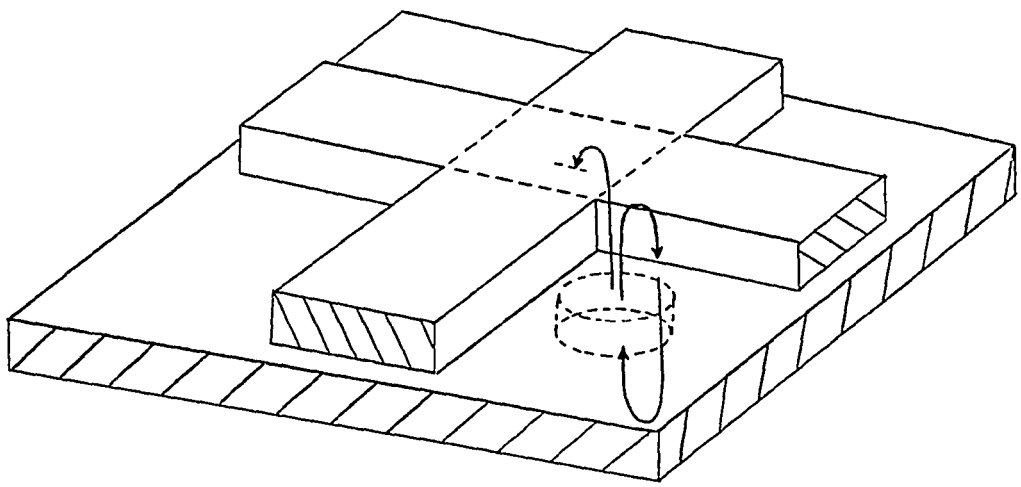

Fig. 23. Schematic drawing of a thin-film Hall probe on the surface of a plate of ferromagnetic material. A reversal in magnetization in the volume shown will produce a field in the active area of the probe (dashed square) which is opposite in sense to the field which would be produced if the same volume were located directly under the active probe area.

magnetization changes in material under the probe and the same types of changes in adjacent material.

Estimation of the Volume of Magnet Material Associated with a Single Barkhausen Step

Although a precise calculation of the volume associated with one of the Barkhausen steps of Fig. 22 would be very difficult due to non-uniform fields through the probe, an estimate can be made with the following simplifying assumptions: (1) the magnetization within the sample under the probe is initially M_s, where M_s is the saturation magnetization of the magnet material; (2) the magnetization within the reversed volume of material is $-M_s$; (3) the fields produced in the active volume of the Hall probe are uniform and perpendicular to the probe surface; and (4) the reversal takes place in a strip of material on the surface of the sample as shown in Fig. 24a.

To determine how the voltage of the Hall probe will change when the field in the strip of Fig. 24a is reversed, we can picture the active area of the probe as a series of batteries (Fig. 24b). This is consistent with Eq. 4. Reversing the field within a strip on the probe corresponds to reversing one of the batteries of Fig. 24b. By this analysis, it can be shown that reversing the field within a strip whose width is a fraction x of the total width of the active probe area reduces the Hall voltage by $2xV_i$ where V_i is the

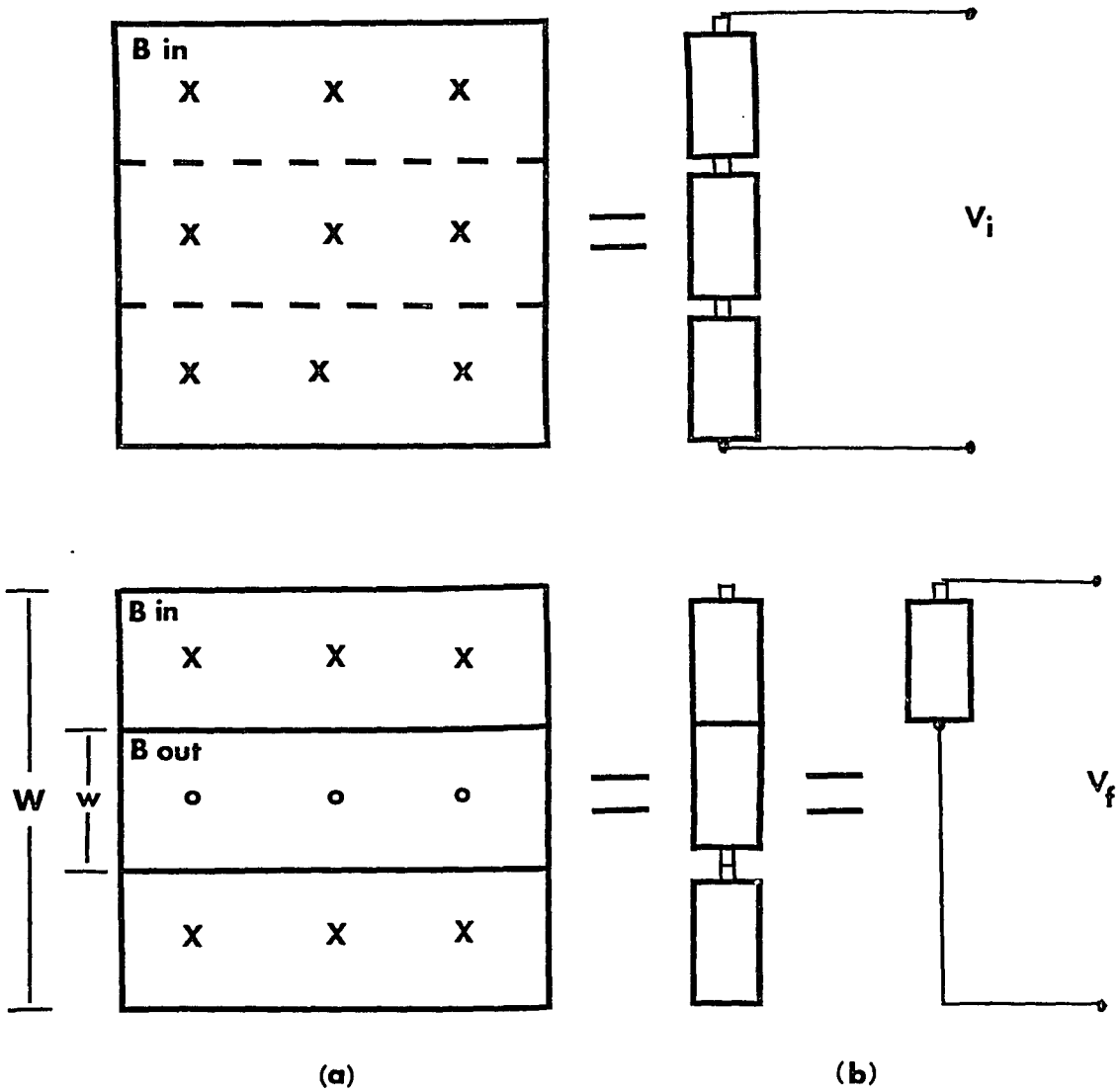

Fig. 24. Battery analog for a Hall probe. In order to determine the amount of magnetic material associated with the Barkhausen steps of Fig. 22, the magnetization reversal is assumed to take place in a strip of material under the active area of the probe (a). Probe current is flowing parallel to the strip. With this arrangement the probe area can be thought of as a series of batteries (b). The voltage change when the magnetization in the strip reverses is $2xV_i$, where $x = w/W$.

initial voltage of the probe, before the reversal has taken place.

The largest voltage step in Fig. 22 corresponds to about one half of the voltage produced by the fully magnetized sample. Since this largest step is positive, the reversal must have occurred under the probe. By the analysis above, this step corresponds to the reversal of a strip of material which is one quarter of the 75 μm width of the probe or about 19 μm. Assuming a depth equal to the width, the volume of material associated with the largest step in Fig. 22 is equal to 19 μm x 19 μm x 75 μm = 2.71×10^4 μm^3. Since the grains of the Nd-Fe-B permanent magnet sample are about 10 μm in diameter (Fig. 25), the step corresponds to the reversal of magnetization in about a half dozen grains (assuming spherical grains). This result contrasts with reports that magnetization steps in Nd-Fe-B magnets at low temperatures are associated with volumes on the order of that of a single grain (Hadjipanayis and co-workers, 1985).

Domain observations in $SmCo_5$ sintered magnets using the Kerr effect have connected Barkhausen steps in the magnetization curve with the reversal of groups of adjacent grains (den Broeder and Zijlstra, 1976). Also, it has been suggested that domain walls can move, sometimes unimpeded, across grain boundaries in sintered $SmCo_5$ magnets (Strnat and co-workers, 1984). It is likely that the larger Barkhausen steps described above for Nd-Fe-B magnets are

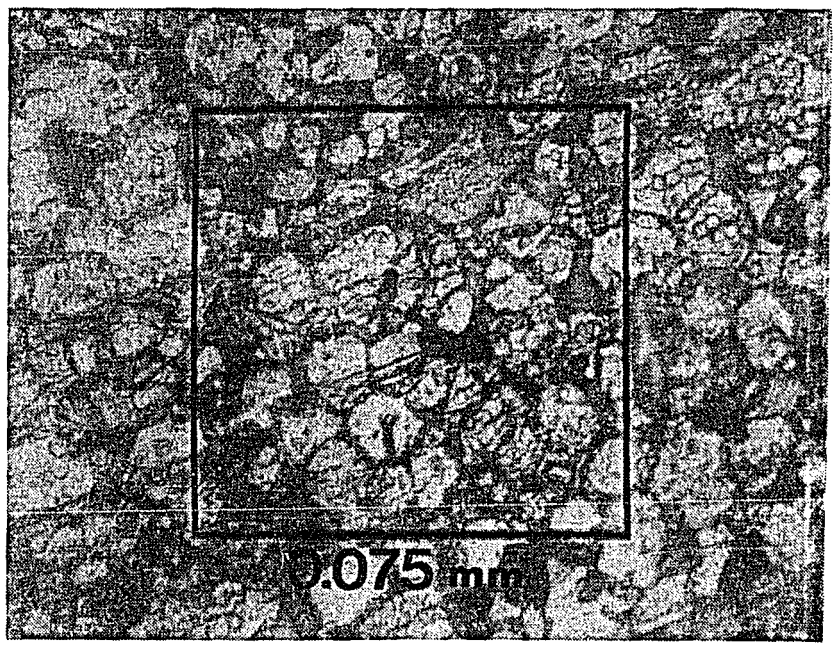

Fig. 25. Photomicrograph of a sample of the Nd-Fe-B magnet which was polished and etched in 2% Nital. The square represents the active probe area.

also associated with the simultaneous reversal of magnetization in several grains, perhaps by the movement of domain walls across grain boundaries. Suzuki and Hiraga (1986) found that domain walls can extend into the grain boundary regions in Nd-Fe-B magnets, indicating that traversal of a grain boundary by a domain wall is possible. It must be pointed out, however, that reversal of domains in adjacent grains may also occur by the purely magnetostatic interaction between such domains.

Cyclic Magnetization of Initially Demagnetized Specimens in Fields of Increasing Amplitude

Hall traces of the magnetization of a thermally demagnetized sample of the Nd-Fe-B magnet are shown in Fig. 26. (Again, the applied field was increased or decreased at a rate of approximately 50 mTs^{-1}.) In this case the maximum applied field was increased on each half cycle of magnetization. On returning the applied fields to zero, the traces in general did not contain measurable Barkhausen steps so these traces are not included in the figure.

After each pair of traces (1,2), (3,4) etc. were recorded the pen on the chart recorder was moved down to avoid overlapping the traces. This has the effect of shifting the zero on the Hall-voltage axis after each even numbered trace, however the relationship between the traces within a pair is retained. For example, after trace 9 in Fig. 26 was recorded and the applied field turned off, the

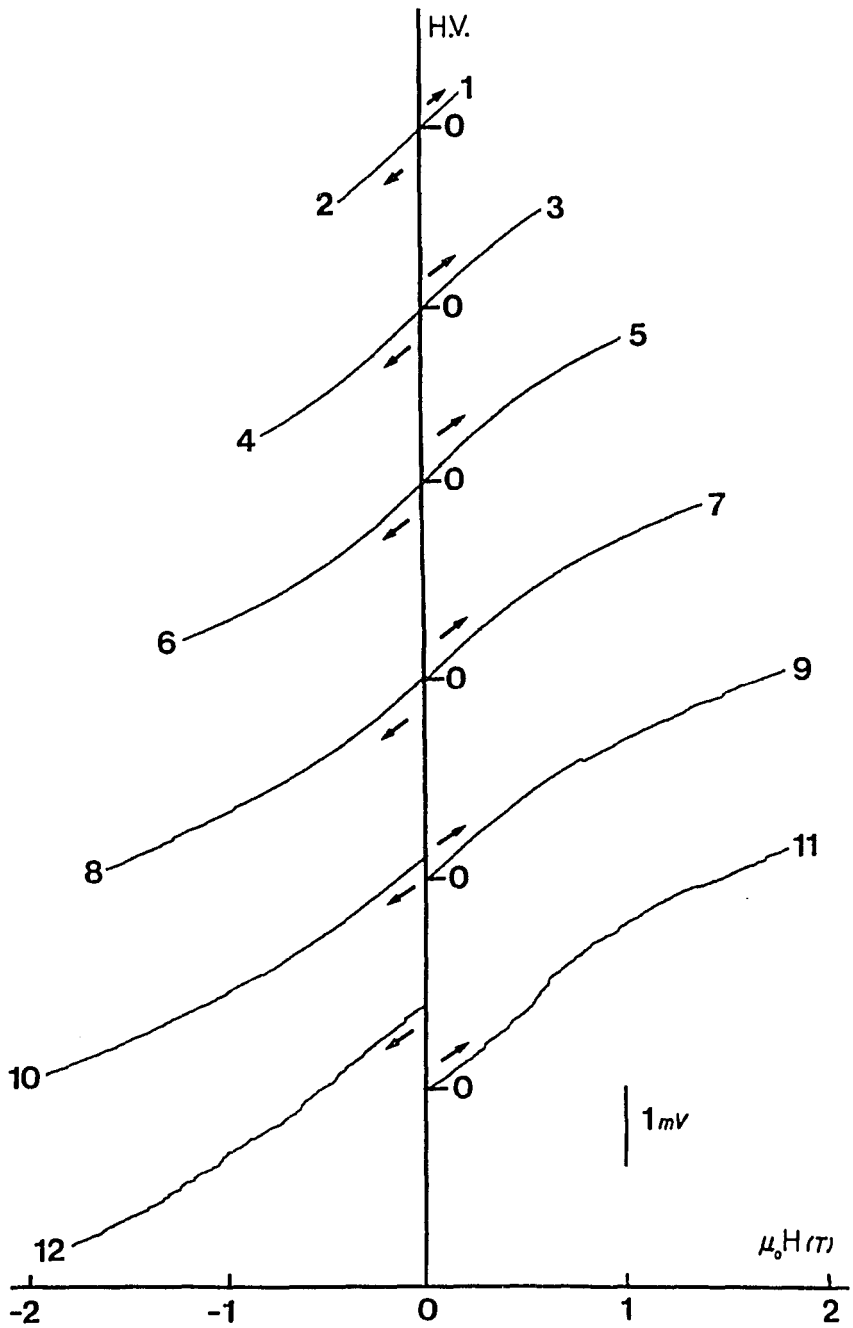

Fig. 26. Hall voltage traces produced by cyclic magnetization of a thermally demagnetized sample of the Nd-Fe-B magnet. Only the traces for increasing field magnitude are given. The zero on the Hall voltage scale was shifted after each pair of traces was recorded. A -2.5 T pulse was applied before trace 11 and a +2.5 T pulse before trace 12.

pen came to rest where trace 10 starts at the H.V. axis. The displacement of this point from the beginning of trace 9 is a result of the remanent magnetization in the sample. As shown in the figure, the remanent magnetization tends to increase as the maximum applied field increases. The large displacement between traces 11 and 12 is a result of a large remanent induction caused by applying a -2.5 T pulse before trace 11 and a +2.5 T pulse before trace 12. These large-field pulses also have the effect of increasing the number of Barkhausen steps which occur in the traces. This effect is a result of the unpinning of domain walls which became pinned in the strong fields.

The traces of Fig. 26 show that Barkhausen steps are present in the traces only after rather large fields have been previously applied; however the steps themselves can occur in low fields. It appears that domain walls become pinned under large fields but can be unpinned relatively easily in some cases. Thus the efficiency of pinning may not be directly related to the strength of the maximum applied field. Again because of the magnitude of the steps observed, it is supposed that domain reversals in several nearby grains occur simultaneously.

Cyclic Magnetization of Initially Demagnetized Specimens in Fields of Constant Amplitude

Hall traces generated from the cyclic magnetization of thermally demagnetized samples of the Nd-Fe-B magnet are

shown in Figs. 27 and 28. Again only the traces from fields of increasing magnitude are given and the zero on the Hall-voltage scale was readjusted after each pair of traces was produced.

As expected, the virgin magnetization traces in Figs. 27 and 28 do not display any features (because of easy domain wall movement through the interiors of grains), however all succeeding traces do. It is interesting to note that many more Barkhausen steps occur upon initial demagnetization (labeled 2 in each figure) than on subsequent traces. This phenomenon can be explained on the basis of domain walls becoming more efficiently pinned at grain boundaries after the first cycle of magnetization. An interesting feature in Fig. 28 is indicated with an arrow. This Barkhausen step developed after two cycles and appeared to repeat at the same field on subsequent demagnetization traces. It appears that a domain wall is becoming pinned and unpinned in a cyclic way. Similar repeating events of lesser magnitude occur in the forward (even numbered) magnetization traces in Figs. 27 and 28. This behavior was mentioned by Li and Strnat (1985) who observed by Kerr-effect microscopy that spike-shaped domains in Nd-Fe-B can suddenly pop into equilibrium size and be made to disappear in a repeatable fashion by reversing and re-reversing the applied field.

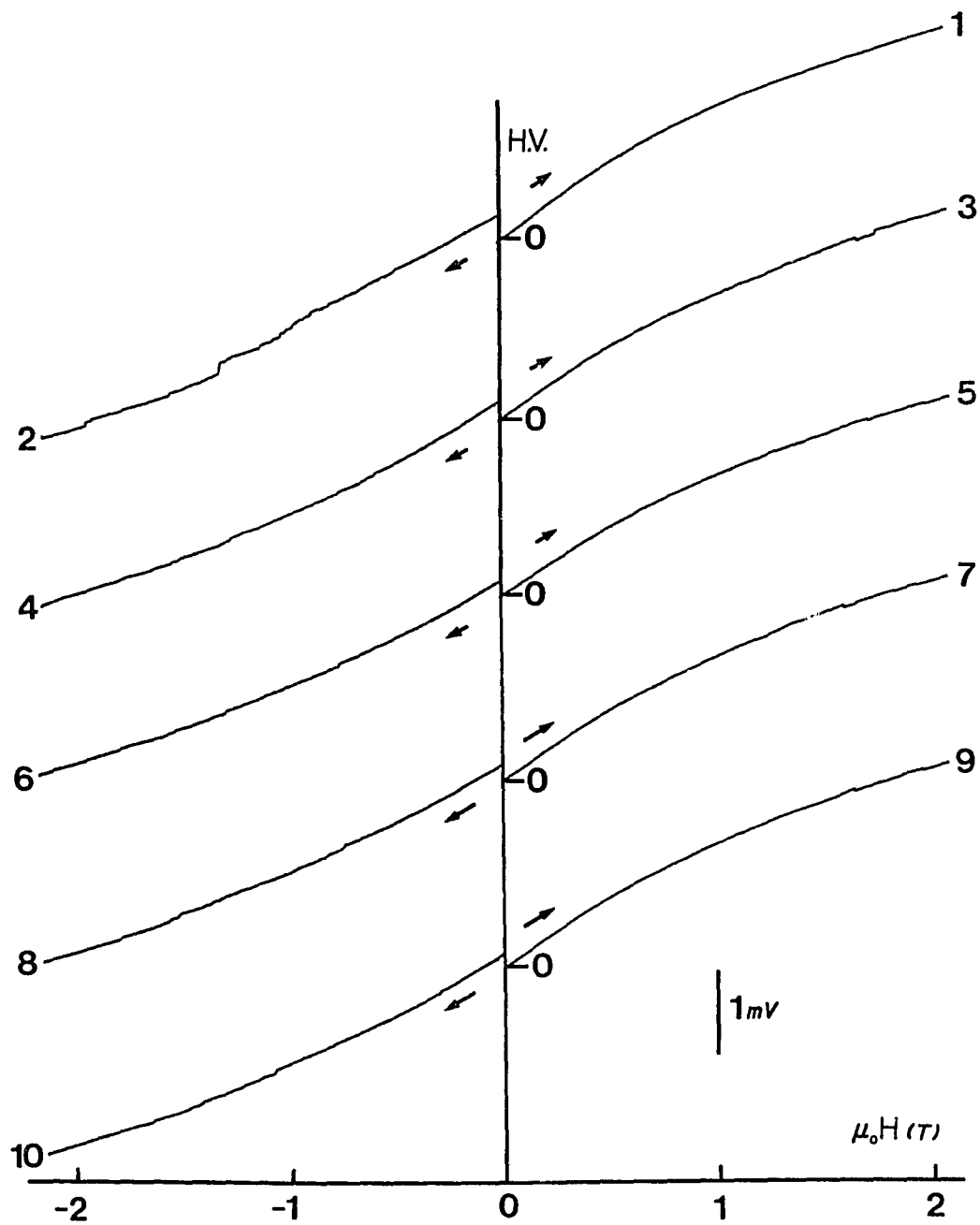

Fig. 27. Hall voltage traces produced by cyclic magnetization of a thermally demagnetized sample of the Nd-Fe-B magnet. The zero on the Hall voltage scale was shifted after each pair of traces was recorded.

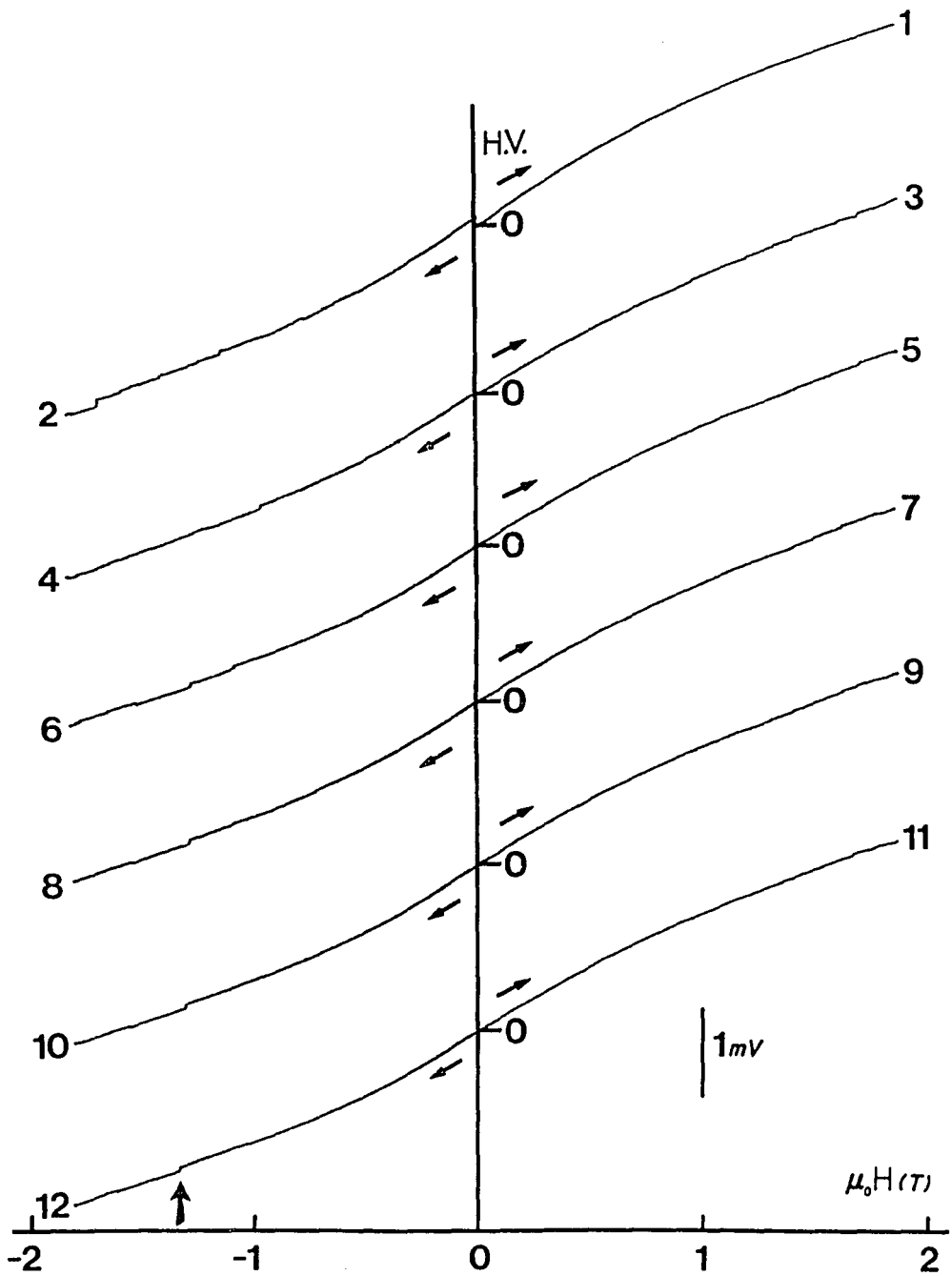

Fig. 28. Hall voltage traces produced by cyclic magnetization of a second thermally demagnetized sample of the Nd-Fe-B magnet. The zero on the Hall voltage scale was shifted after each pair of traces was recorded.

Comparison of Results of the Present Investigation with Previous Investigations of Magnetization Changes in Nd-Fe-B Magnets

The Hall-voltage traces of Figs. 22, 26, 27, and 28 can be directly correlated with conventional magnetic measurements on Nd-Fe-B magnets and domain observations in this material. The connection is made by analysis of the Barkhausen steps contained in the traces. For example, the absence of Barkhausen steps in the virgin magnetization traces of Figs. 27 and 28 is directly related to the ease of domain wall motion through the defect-free interiors of grains as established by Livingston (1985) and Li and Strnat (1985) by Kerr-effect microscopy. This fact was also established by Sagawa and co-workers (1984a) by conventional magnetic measurements. Table 4 is a list of observations of domain behavior made by Li and Strnat (1985) utilizing the Kerr effect (which is considered to be the most detailed investigation of its type) along with related observations made by conventional magnetic measurements. In the next column, the characteristics of the Hall-voltage traces which are related to the observations in the first column are given.

One very interesting observation of Li and Strnat (1985) is the apparent "nucleation" of spike-shaped domains at grain boundaries. The authors reported that the "nuclei" of these domains could be made to grow only if the original nucleation field was applied and that growth occurred by

Table 4. Comparison of Results of the Present Investigation with Results of Previous Investigations of Magnetization Changes in Nd-Fe-B Magnets

Previous Investigations	Present Work
Sagawa and co-workers (1984a) detected a steep rise in the virgin magnetization curve in Nd-Fe-B magnets and Livingston (1985) and Li and Strnat (1985) observed by Kerr-effect microscopy that domain walls can move easily through the interiors of $Nd_2Fe_{14}B$ grains.	Hall traces generated during the virgin magnetization of Nd-Fe-B magnet samples do not contain Barkhausen steps. This indicates that domain wall motion is not impeded by pinning sites within grains.
* * *	* * *
Sagawa and co-workers (1984a) found that the intrinsic coercivity of Nd-Fe-B magnets is dependent on the maximum magnetizing field and Li and Strnat (1985) observed by Kerr-effect microscopy that spike-shaped domains "nucleate" at grain boundaries and suddenly pop into equilibrium size when a sample which was magnetized in a sufficiently large field is demagnetized.	Hall traces of cyclically-magnetized Nd-Fe-B samples show that Barkhausen steps, indicative of the unpinning of domain walls and rapid domain wall motion, do not occur until a large enough magnetizing field has been applied. This suggests that the effectiveness of domain-wall pinning is increased as the applied field increases.
* * *	* * *

Table 4, Continued

Previous Investigations	Present Work
Li and Strnat (1985) observed by Kerr-effect microscopy that spike-shaped domains which "nucleate" at grain boundaries can be removed by reversing the field direction. If suppression field is large enough the same "nuclei" can be made to grow only if the original nucleation field is applied.	Hall traces produced during cyclic magnetization of Nd-Fe-B samples contain Barkhausen steps which repeat at the same field, cycle after cycle. This indicates that the formation of some reverse domains, either by nucleation or unpinning of domain walls, is a repeatable process.
* * *	* * *
Hadjipanayis and co-workers (1985) reported that magnetization steps in Nd-Fe-B magnets at low temperatures are associated with volumes on the order of that of a single grain	The magnitude of some individual Barkhausen steps in the Hall-voltage traces are too large to be associated with the magnetization reversal in a single grain. This means that the simultaneous reversal in several adjacent grains probably occurs.
however	
Strnat and co-workers (1984) found, by Kerr-effect microscopy, that domain walls can move across grain boundaries in $SmCo_5$ magnets.	* * *
	Hall traces generated during cyclic magnetization of Nd-Fe-B samples are not the same on each subsequent magnetization cycle. This suggests that pinning is an important coercivity mechanism in Nd-Fe-B magnets at least for fields below 2 T.

sudden popping into equilibrium size. The sudden expansion of domain walls at certain well defined fields is recorded in the repeating Barkhausen steps of Figs. 27 and 28.

These apparent nucleation events give credence to theories which consider the nucleation of reverse domains to be the dominant coercivity mechanism in Nd-Fe-B magnets. However, as stated by Livingston (1981) it is difficult to distinguish between a true nucleation event and the breaking free of a small persistent domain wall which was pinned at a grain boundary. From the practical point of view of making better magnets this is the all important question. If a pure nucleation mechanism is operating, one would want to reduce the number of defects at grain boundaries to a minimum. However if domain-wall pinning is important, the opposite may be true.

The traces of Figs. 27 and 28 show that although nucleation of reverse domains may occur in Nd-Fe-B magnets, nucleation is not the only important coercivity mechanism. If it were, the traces made after the first cycle should be identical; that is, nucleation of a specific domain should occur at the same field regardless of the magnetization history. However, if wall pinning is operating, the final configuration of the trapped wall may take several magnetization cycles to develop as the Hall traces appear to show.

Livingston (1981) reported that domain-wall pinning at grain boundaries is essential even in a

nucleation-controlled magnet, otherwise a single defect could cause an entire macroscopic magnet to reverse its state of magnetization. It appears that both nucleation (including the breaking free of small persistent domains as nucleation events) and wall pinning occur in Nd-Fe-B magnets. The sources of nucleation and/or pinning of domain walls remain to be determined.

CHAPTER 6

CONCLUSIONS

Hall microprobe measurements during the magnetization of samples of a Nd-Fe-B permanent magnet have yielded information regarding the domain behavior in the material. The results of the investigation can be summed up as follows.

1. Hall voltage traces for the demagnetization of fully magnetized samples contain Barkhausen steps indicative of rapid domain reversals in small volumes of the material. It is likely that the largest steps correspond to the nearly simultaneous reversal of domains in several nearby grains rather than a single grain.

2. Barkhausen steps in the magnetization of thermally demagnetized samples of the Nd-Fe-B magnet were only observed in the traces after rather large fields (approximately 1.2 T) were applied; however the steps themselves can occur in lower fields.

3. Hall voltage traces made during the virgin magnetization of thermally demagnetized samples are smooth, exhibiting no Barkhausen steps.

4. The first demagnetization trace following virgin magnetization exhibits Barkhausen steps which are in general

larger in number and magnitude than those on subsequent cycles.

5. Finally, in some cases, Barkhausen steps which occurred after one or two cycles of magnetization became repeatable--occurring at nearly the same field on each subsequent forward or reverse trace.

REFERENCES

Becker, J. J. (1969). IEEE Trans. Magn. MAG 5 (3), 211.

Becker, J. J. (1971). IEEE Trans. Magn. MAG 7, 644.

Becker, J. J. (1975). AIP Conf. Proc. 24, 676.

Becker, J. J. (1976). IEEE Trans. Magn. MAG 12 (6), 965.

Becker, J. J. (1984). J. Appl. Phys. 55 (6), 2067.

Bozorth, R. M. and Dillinger, J. F. (1931). Nature 127 (3212), 777.

Bozorth, R. M. (1951). Ferromagnetism, D. Van Nostrand Co., Toronto.

Brown, W. F. (1963). Micromagnetics, Interscience Publishers, New York.

Buschow, K. H. J., Naastepad, R. A., and Westendorp, F. F. (1969). J. Appl. Phys. 40, 4029.

Croat, J. J. and Herbst, J. F. (1982). J. Appl. Phys. 53 (3), 2404.

Croat, J. J. (1982). J. Appl. Phys. 53 (3), 3161.

Croat, J. J., Herbst, J. F., Lee, R. W., and Pinkerton, F. E. (1984). J. Appl. Phys. 55 (6), 2078.

Das, D. K. (1969). IEEE Trans. Magn. MAG 5 (3), 214.

den Broeder, F. J. A. and Zijlstra, H. (1975). J. Appl. Phys. 47 (6), 2688.

Dillon, J. F. (1963). Magnetism Vol. III, Academic Press, New York.

Fidler, J. (1981). Proceedings of the Fifth International Workshop on Rare Earth-Cobalt Permanent Magnets and their Applications, University of Dayton, Dayton Ohio.

Fidler, J. (1985). IEEE Trans. Magn. MAG 21, 1955.

Hadjipanayis, G. C., Hazelton, R. C., and Lawless, K. R. (1984). J. Appl. Phys. 55 (6), 2073.

Hadjipanayis, G. C., Lawless, K. R., and Dickerson, R. C. (1985). J. Appl. Phys. 57 (1), 4097.

Handstein, A., Schneider, J., Stephan, D., Fisher, W., Heinecke, U., Grossinger, R., Sassik, H., and Kirchmayr, H. R. (1985). Materials Letters 3 (5,6), 200.

Herbst, J. F., Croat, J. J., Pinkerton, F. E., and Yelon, W. B. (1984). Phys. Rev. 29 (7), 4176.

Hiraga, K., Hirabayashi, M., Sagawa, M., and Matsuura, Y. (1985). Jpn. J. Appl. Phys. 24 (1), L30.

Hoffer, G. and Strnat, K. (1966). IEEE Tran. Magn. MAG 2 (3), 487.

Hubbard, W. M., Adams, E., and Gilfrich, J. V. (1960). J. Appl. Phys. 31 (5), 368S.

Kittel, C. (1976). Introduction to Solid State Physics, John Wiley and Sons, New York.

Koon, N. C. and Das, B. N. (1984). J. Appl. Phys. 55 (6), 2063.

Kostyshyn, B., Brophy, J. E., Oi, I., and Roshon, D. D. (1960). J. Appl. Phys. 34, 637.

Li, D. and Strnat, K. J. (1985). J. Appl. Phys. 57 (1), 4143.

Liu, S., Strnat, K. J., and Mildrum, H. F. (1982). Proceedings of the Sixth International Workshop on Rare Earth-Cobalt Permanent Magnets and their Applications, Druckerei Lischkar and Co., Vienna, Austria.

Livingston, J. D. (1973). AIP Conf. Proc. 10, 643.

Livingston, J. D. (1981). J. Appl. Phys. 52 (3), 2544.

Livingston, J. D. (1985). J. Appl. Phys. 57 (1), 4137.

Luborsky, F. E. (1961). J. Appl. Phys. 32 (3), 171S.

Mayer, L. (1957). J. Appl. Phys. 28 (9), 975.

McCaig, M. (1977). Permanent Magnets in Theory and Practice, Halsted Press, New York.

McCurrie, R. A. (1970). Phil. Mag. 22, 1013.

McCurrie, R. A. and Mitchell, R. K. (1975). IEEE Trans. Magn. MAG 11 (5), 1408.

Menth, A., Nagle, H., Perkins, R. S. (1978). Ann. Rev. Materials Science, Huggins, R. A., Bube, R. H., and Roberts, R. W., eds. 8, 21.

Nesbitt, E. A., Wernick, J. H., and Corenzwit, E. (1959). J. Appl. Phys. 30 (3), 365.

Nesbitt, E. A., Williams, H. J., Wernick, J. H., and Sherwood, R. C. (1962). J. Appl. Phys. 33 (5), 1674.

Nesbitt, E. A. and Wernick, J. H. (1973). Rare Earth Permanent Magnets, Academic Press, New York.

Roshon, D. D. (1962). Rev. Sci. Instr. 22, 201.

Sagawa, M., Fujimura, S., Togawa, H., Yamamoto, H. and Matsuura, Y. (1984a). J. Appl. Phys. 55 (6), 2083.

Sagawa, M., Fujimura, S., Yamamoto, H. and Matsuura, Y. (1984b). IEEE Trans. Magn. MAG 20 (5), 1584.

Sellmyer, D. J., Ahmed, A., Muench, G. and Hadjipanayis, G. (1984). J. Appl. Phys. 55 (6), 2088.

Shoemaker, C. B., Shoemaker, D. P., and Fruchart, R. (1984). Acta. Cryst. C40, 1665.

Stadelmaier, H. H., Elmasry, N. A., Liu, N. C. and Cheng, S. F. (1984). Materials Letters 2 (5), 411.

Strnat, K. J., Hoffer, G., Olsen, J., Ostertag, W., and Becker, J. J. (1967). J. Appl. Phys. 38, 1674.

Strnat, K. J., Li, D., and Mildrum, H. F. (1984). J. Appl. Phys. 55 (6), 2100.

Suzuki, T. and Hiraga, K. (1986). J. Magn. Magn. Mat. 54-57, 527.

Tiesong, Z., Hanmin, J., Jingcuan, D., Fengwen, W., Jihua, S., and Yan, S. (1986). J. Magn. Magn. Mat. 54-57, 573.